2016

Long-Term Patterns of Air Temperatures, Daily Temperature Range, Precipitation, Grass-Reference Evapotranspiration and Aridity Index in the Usa Great Plains: Part I. Spatial Trends

Meetpal S. Kukal
University of Nebraska-Lincoln, meetpal.kukal@unl.edu

Suat Irmak
University of Nebraska-Lincoln, sirmak2@unl.edu

Published in Journal of Hydrology, Vol. 542, pp. 953–977, 2016.

LONG-TERM PATTERNS OF AIR TEMPERATURES, DAILY TEMPERATURE RANGE, PRECIPITATION, GRASS-REFERENCE EVAPOTRANSPIRATION AND ARIDITY INDEX IN THE USA GREAT PLAINS: PART I. SPATIAL TRENDS

M. Kukal and S. Irmak*

University of Nebraska-Lincoln, 239 L.W. Chase Hall, Lincoln, NE.

*Corresponding author (Suat Irmak). Address:
University of Nebraska-Lincoln. 239 L.W. Chase Hall, Lincoln, NE 68583.
Tel.: (402) 472-4865. E-mail address: *sirmak2@unl.edu*.

The mention of trade names or commercial products is for the information of the reader and does not constitute an endorsement or recommendation for use by the authors or their institution.

Abstract*: Due to their substantial spatio-temporal behavior, long-term quantification and analyses of important hydrological variables are essential for practical applications in water resources planning, evaluating the water use of agricultural crop production and quantifying crop evapotranspiration patterns and irrigation management vs. hydrologic balance relationships. Observed data at over 800 sites across the Great Plains of USA, comprising of 9 states and 2,307,410 km^2 of surface area, which is about 30% of the terrestrial area of the USA, were used to quantify and map large-scale and long-term (1968-2013) spatial trends of air temperatures, daily temperature range (DTR), precipitation, grass-reference evapotranspiration (ET_o) and aridity index (AI) at monthly, growing season and annual time steps. Air temperatures had a strong north to south increasing trend, with annual average varying from -1 to 24°C, and growing season average temperature varying from 8 to 30°C. DTR gradually decreased from western to eastern parts of the region, with a regional annual and growing season averages of 14.25℃ and 14.79℃, respectively. Precipitation had a gradual shift towards higher magnitudes from west to east, with the average annual and growing season (May-September) precipitation ranging from 163 to 1,486 mm and from 98 to 746 mm, respectively. ET_o had a southwest- northeast increasing trend, with regional annual and growing season averages of 1,297 mm and 823 mm, respectively. AI increased from west to east, indicating higher humidity (less arid) towards the east, with regional annual and growing season averages of 0.49 and 0.44, respectively. The spatial datasets and maps for these important climate variables can serve as valuable background for climate change and hydrologic studies in the Great Plains region. Through identification of priority areas from the developed maps, efforts of the concerned personnel and agencies and resources can be diverted towards development of holistic strategies to address water supply and demand challenges under changing climate. These strategies can consist of, but not limited to, advancing water, crop and soil management, and genetic improvements and their relationships with the climatic variables on large scales.* ***Keywords.*** *Climate variables, air temperature, daily temperature range, evapotranspiration.*

INTRODUCTION

A wide array of biotic and abiotic processes are characterized by the interactions of climatic variables with the plant environment and hence, a variety of disciplines such as hydrology, agricultural sciences and engineering, agronomy, forest management, ecology, etc. have an important need for spatial information about climatological data to better evaluate and understand the processes that have an impact in their respective areas. Traditionally, this information is obtained from the meteorological stations. However, the available information is usually limited to discrete points in space and the spatial density and coverage of these sites is not sufficient, which limits the applicability of the information. The density of the weather stations is of high importance to the professionals who rely on point data as inputs to various models in a range of subjects. The success and accuracy of point-based simulations are affected by the availability of observational datasets in proximity of the location studied. Owing to the sparsely installed observational networks, the stations can be as far as tens or hundreds of kilometers from each other. This important weakness of the climate networks would consequently result in the likelihood that the nearest available data might not be representative of the conditions at the location of interest. Besides a variety of applications in point-based simulations, accurate and reliable estimates of climate variables on a spatial scale are a prerequisite for the effective and efficient modeling of a wide range of environmental processes. Variables such as air temperature and precipitation, when studied on a geographical scale, are instrumental in understanding the spatial variation that occurs in many processes in a particular region. For this reason, it is crucial to develop and compile detailed maps to accurately understand spatial as well as temporal variation in meteorological variables. Continuous surfaces of a variety of climate variables using point based information have been developed for areal extents, ranging from a few thousand kilometers (Holdaway, 1996) to the continental scale (Hulme et al., 1995, 1996; Wilmott and Matsuura, 1995) and even for the entire globe (Wilmott and Robeson, 1995).

The climatic variables addressed in this study are maximum and minimum air temperatures, daily temperature range, precipitation, grass-reference evapotranspiration (ET_o) and aridity index (AI).

Numerous attempts have been made to use various techniques in order to map these variables for different regions around the globe. Air temperature is one of the major factors in crop development, crop water stress, yield potential and crop water use, because of the strong interrelationship between crop production and temperature (Skaggs and Irmak, 2012). It is one of the main input data for numerous models such as agrometeorological models for water balance monitoring, hydrological models and crop models for yield prediction. For instance, plant growth is a function of air temperature and hence, crop models rely on accumulated air temperatures since sowing to determine the crop phonological stages. For these reasons, it is necessary to have reliable spatial estimates of the air temperature data (e.g., in the form of maps). Moreover, it is a very well established fact that quantifications of average temperatures (and other averaged variables) are not sufficient in full understanding of the implications of weather or climate on agriculture. Due to erratic sensitivity of agriculture to weather variables in various crops and crop development stages, it becomes necessary to map these variables on various temporal scales other than annual basis such as agricultural growing season and different months of the year. Various researchers have used various interpolation techniques to carry out this exercise in various parts of the globe. Courault and Monestiez (1999) proposed a methodology of spatial interpolation of air temperature, taking into account the effect of circulation patterns, for Southeast France. Dodson and Marks (1997) compared various interpolation methods to map daily air temperature at high spatial resolution over a large mountainous area in the Columbia River Basin. Similarly, Kurtzman and Kadmon (1999) mapped temperature variables using various interpolation methods in Israel. Ninyerola (2007) conducted objective air temperature mapping for the Iberian Peninsula, Europe, using spatial interpolation and GIS techniques.

Precipitation, which is a major driver of many processes and an indispensable component of the water balance, can be extremely variable in both time and space. Quantification of its spatial variability in any region is important to understand its potential implications on water resources and crop production. The variability that occurs in precipitation amounts in various seasons drives the soil water availability to a great extent and strongly influences crop productivity and hydrologic balances. Conditions arising due

to excess or lower precipitation amounts, lead to issues such as drainage concerns and imposition of stress on water resources in agricultural areas. This justifies the need of mapping precipitation amounts for any agro-ecosystem at various temporal scales, especially for the agricultural growing season months, to understand its potential impact on the crop performance. Similar to air temperatures, there are various studies that focused on precipitation mapping using spatial interpolation. For example, Sharma and Irmak (2012) compared two interpolation methods and developed long-term averaged maps for annual and growing season precipitation and investigated spatial precipitation trends in Nebraska, USA.

Another important variable studied spatially and temporally in this research is reference evapotranspiration (ET_o), which is one of the indicators of atmospheric water demand from a reference crop surface, is an important variable for quantification of crop water use. Evapotranspiration is an important parameter in every local or regional scale project which include hydrologic components, irrigation management, water resources planning and land use development vs. water resources relationships. Many ET_o estimation equations use air temperature as one of the primary driver of ET (Penman, 1948; McCloud, 1955; Turc, 1961; Monteith, 1965; McGuinness and Bordne, 1972; Doorenbos and Pruitt, 1977; Mather, 1978). ET_o maps at various temporal scales (especially on a growing season basis) prove to be instrumental in providing valuable information for management of cropping systems on a regional area, delineation of agro-climate divisions and monitoring agricultural water use on a spatial scale. Numerous studies exist in the literature, which aimed at quantification and mapping of ET_o for different regions. Similar to precipitation, Sharma and Irmak (2012) mapped alfalfa-reference ET (ET_r) for Nebraska using Penman-Monteith reference ET equation.

Spatial surfaces of AI, which relates both precipitation and ET_o, can be instrumental in providing information about drought/wetness regimes present in a given region. Also, it is possible that arid and semi-arid regions may be more vulnerable to effects of changing climate than the humid regions. Consequently, a deep understanding of aridity is a prerequisite to explain landscape characteristics and to plan rational utilization of water resources. This emphasizes the need of delineation of aridity classes for

the region. Since the distribution of both precipitation and ET_o is variable for different months of the year, development of monthly AI maps would be valuable to observe the month-specific dryness or wetness that might be prevalent in the area. Most importantly, consideration of growing season AI would be very important to evaluate its potential impacts on agricultural applications. Thus, the primary objectives of this study were to quantify spatial variability in air temperatures, precipitation, ET_o and AI over the USA Great Plains and establish basic ground work and analyses to carry out temporal trend investigations on a county basis and analyze the spatial distribution of temporal trends. The specific objectives were to quantify (where applicable) and map regional scale air temperatures, daily temperature range, precipitation, ET_o and AI for the USA Great Plains over a 46-year period (1968-2013) and quantify, map and analyze the spatial patterns and geographical distribution for each of the variables at monthly, growing season (May-September) and annual time steps. The Part II of this study (Kukal and Irmak, 2016) uses the spatial datasets of the aforementioned climatic variables developed in this current study (Part I) to extract zonal (countywide) values to investigate temporal trends during the period from 1968 to 2013.

MATERIALS AND METHODS

STUDY AREA DESCRIPTION

This study covers the central USA region, which is generally designated as the Great Plains (Figure 1). The marginal areas of the region extend from the Canadian border in the north to Texas in the south, Wyoming and Colorado on the west and Iowa on the east. Specifically, the area consists of nine states (North Dakota, South Dakota, Nebraska, Iowa, Wyoming, Colorado, Kansas, Oklahoma and Texas), which together comprise of 834 counties. The total land area enclosed by these states is 2,307,410 km^2, which is about 30% of the terrestrial area of the USA. The area lies between dense forests on the east and mountains and deserts on the west (Rossum and Lavin, 2000). The topographical characteristic of the area are the vast, flat-to-rolling plains. The highest elevation throughout the region is in the Rocky

Mountains in Colorado and the lowest elevation is at the southern coastline in Texas. Temperature and precipitation have an evident north-south and east-west gradient, respectively. The long-term average (1968-2013) annual precipitation ranges from 215 mm in the west to 1,450 mm in the southeast. Similarly, long-term average (1968-2013) growing season (1 May to 30 September) precipitation varies from 120 mm in the west to 700 mm in the southeast. The long-term average (1968-2013) annual maximum and minimum air temperature varies from 9°C in the north to 30°C in the south and -6°C in the north to 18°C in the south, respectively. The cold air fronts from Canada in the north and Rocky Mountains in the northwest along with warm and humid air masses flowing into the region from Gulf of Mexico from the south govern the climatic conditions of the region (Irmak, 2010; Irmak et al., 2012). This highly variable climatic behavior is evident from the fact that the region is divided into 78 climatic divisions by NOAA. The major land use categories that fall in the region are primarily agricultural, including rangelands, prairies, irrigated and rainfed farming of agronomic row crops such as maize, soybean, sorghum, alfalfa, winter wheat, sugar beets and cotton (Mutiibwa and Irmak, 2013). In the eastern parts, mostly non-irrigated crop production is practiced, whereas in the western parts irrigated crop production is dominant. The major source of irrigation is the Ogallala aquifer (Rosenberg et al., 1999).

INPUT DATA SOURCES

The primary dataset used in this study is the daily weather dataset consisting of maximum air temperature, minimum air temperature and precipitation. The source for the dataset is the Global Historical Climatology Network (GHCN) provided through the National Climatic Data Centre-National Oceanic and Atmospheric Administration (NCDC-NOAA). The GHCN dataset is subjected to rigorous quality assurance reviews. Historical daily weather datasets for the period 1968-2013 were obtained for over 800 weather stations distributed over the study area. The selection is performed so that all the weather stations selected possess regular data during the temporal span of 46 years. Out of these sites, 672 sites are geographically situated in the 9 aforementioned states. The rest of the sites are selected from the

surrounding states along the boundaries of the study area, specifically in the states of Arkansas, Idaho, Illinois, Louisiana, Missouri, Montana, Minnesota, New Mexico, Utah and Wisconsin to perform more accurate interpolation of various variables along the edges of the study area. The boundary datasets for various governmental units such as states and counties that were used to aid in the analysis and representation in the GIS environment are obtained from the USDA- Geospatial Data Gateway. The US Climate Divisional Dataset used in the study was obtained from the National Climatic Data Center-National Oceanic and Atmospheric Administration (NCDC-NOAA). Figure 1 represents the visual integration of various datasets such as Digital Elevation Model of the study area, boundary datasets and point locations of the weather station sites.

QUANTIFICATION OF GRASS-REFERENCE ET (ET_o)

The Hargreaves-Samani (HS) equation (Hargreaves and Samani, 1985) that requires only maximum and minimum air temperatures, with extraterrestrial radiation calculated as a function of latitude and day of the year, was used to quantify ET_o. This equation is widely used in regions where meteorological stations providing detailed measurements including all the variables are not available to solve combination-based energy balance equations. The HS ET_o was calculated using Eq. (1) at all 800 sites at a daily time step using:

$$ET_{oHS} = 0.0023\, R_a (T + 17.8)\sqrt{T_{max} - T_{min}} \quad (1)$$

where, ET_{oHS} = grass reference evapotranspiration (mm d^{-1}), T is daily mean air temperature (°C), T_{max} is daily maximum air temperature (°C), T_{min} is daily minimum air temperature (°C), R_a is water equivalent of the extraterrestrial radiation (mm d^{-1}) computed using Eq. (2) and 0.0023 is the original empirical coefficient proposed by Hargreaves and Samani (1985).

$$R_a = \frac{24(60)}{\Pi} G_{sc} d_r \left[\omega_s \sin(\varphi) \sin(\delta) + \cos(\varphi) \cos(\delta) \sin(\omega_s)\right] \quad (2)$$

$$d_r = 1 + 0.033 \cos\left(\frac{2\pi}{365} J\right) \quad (3)$$

$$\delta = 0.409 \sin\left(\frac{2\pi}{365} J - 1.39\right) \quad (4)$$

$$\omega_s = \arccos[-\tan(\varphi)\tan(\delta)] \quad (5)$$

where, *Ra* is extraterrestrial radiation (MJ m^{-2} d^{-1}), G_{sc} is solar constant (0.0820 MJ m^{-2} min^{-1}), d_r is inverse relative distance from earth to sun (Eq.3), ω_s is sunset hour angle (rad) (Eq.5), φ is latitude (rad), δ is solar declination (rad) (Eq. 4).

In this study, a previously developed approach (Kukal et al., 2016), which integrates the Hargreaves-Samani equation with a spatial and temporal calibration strategy, was used to estimate ET_o. Following the computation of daily ET_o using HS equation for the period of 1968-2013, the daily ET_o is summed for each month of each year in this time period, resulting in total monthly ET_o for every month for the period of 46 years. These point estimates of monthly ET_o were interpolated to generate spatial datasets. This procedure resulted in 552 raster surfaces (one raster for each month in a single year).

The HS equation is a temperature-based equation and its use is often accompanied by issues related to overestimation and underestimation of ET_o, depending on the climatic conditions, when compared to combination-based equations such as Penman-Monteith (PM) equation. To address this, previously we assessed the spatio-temporal performance of the original HS equation against the Penman-Monteith (PM) equation at 124 sites geographically distributed over the USA Great Plains (Kukal et al., 2016). The performance of the HS ET_o estimates varied substantially over the region, depending on the climate characteristics under consideration and geographical location of the sites. The HS equation underestimated ET_o at arid, semi-arid and dry sub humid sites and overestimated at humid sites, although there were few sites that showed underestimations. Also, temporal variation in the performance of HS equation was explored. The equation performed better in summer months than the rest of the year at sites in semi-arid and dry sub humid areas. However, at humid sites, the equation showed relatively high

deviations from the PM-estimated ET_o values during the summer months than the remainder of the year. In fact, the humid sites, on an average, during the winter months showed underestimation, similar to semi-arid and dry sub humid areas. The variability in performance of HS equation, both spatially and temporally makes the equation unacceptable to be used for any practical applications without any local calibration. Thus, the HS equation was calibrated using an extensive spatio-temporal calibration coefficient approach. The calibration procedure, performance and validation results on spatial and temporal scales for the study region have been reported in Kukal et al. (2016) and will not be repeated here. However, some of the critical components of the calibration process will be presented. GIS techniques were used to generate spatial surfaces of these calibration coefficients to determine a spatial pattern of magnitude of underestimation and overestimation by the HS equation for each month. The resulting surfaces were used in conjunction with the original HS equation to determine the calibrated ET_o through four different calibration approaches, which varied by the choice of using either annual or monthly rasters or application of zonal or point-based calibration coefficients. All these approaches along with the original HS equation were applied simultaneously on several validation sites and the results were compared against PM equation through a set of statistical indicators (Kukal et al., 2016). At all validation sites, each of the four approaches performed better than the original HS equation. When comparing the four approaches among each other, it was observed that for almost all sites, the point-based calibration resulted in better estimates than the zonal calibration coefficients and the monthly coefficients yielded better estimates than annual coefficients. Hence, it was established that the best strategy to be applied in such data-limited situations is the monthly point-based calibration approach. For this purpose, rasters of monthly calibration coefficients were developed and used with rasters of the original HS monthly ET_o estimates to determine improved estimates of the monthly ET_o for the period of 1968-2013. Finally, the calibrated rasters of monthly total ET_o for the period from 1968 to 2013 were aggregated to develop the annual and growing season (May 1^{st} -Sept 30^{th}) ET_o rasters.

ARIDITY INDEX

There are many formulations to describe an AI (Mannocchi et al., 2004). In this study, the AI index was calculated according to the UNESCO (1979) procedure, which is the ratio of mean annual precipitation over the mean annual ET_o (Eq. 6). UNEP (1997) has laid out classification of the AI, which is presented in Table 1. Using this classification scheme, any region or site can be identified as hyper arid, arid, semi-arid, dry-sub humid and humid categories based upon the magnitude of AI. The mean annual ET_o is obtained for each year in the analyses period (1968-2013) by summing the monthly ET_o rasters. Similarly, annual precipitation is obtained by summing the monthly rasters for each year. Subsequently, the spatial AI raster for each month/year/growing season was obtained by the ratio of spatial precipitation for that period to the spatial ET_o for that period. This procedure resulted in 46 annual spatial datasets, 46 growing season spatial datasets and 552 monthly spatial datasets of AI.

$$Aridity\ Index\ (AI) = \frac{Precipitation}{ET_o} \tag{6}$$

SPATIAL DATASETS

Any variable of interest needs to be represented as a continuous surface rather than point specific values in order to discern and analyze its geographical patterns over a region. In this study, air temperatures, daily temperature range (DTR), precipitation, ET_o and AI also require to be interpolated using point-based measurements or estimates as inputs. The interpolation techniques are usually applied on to a target point-based dataset using various geographical information system tools. In this study, the interpolation process adopted was inverse distance weighing (IDW) and was carried out using the Spatial Analyst Toolset provided in ArcGIS 10.2. IDW is a deterministic interpolation technique, which implies that weights are assigned to point estimates using a mathematical function. The principle behind the IDW technique is that point estimates lying in closer vicinity of the prediction location will be more influential

than the ones farther away. The algorithm followed by the IDW interpolation technique to determine the value of the variable of interest at unknown location ($Z(S_o)$) is:

$$Z(S_o) = \sum_{i=1}^{N} \lambda_i Z(S_i) \tag{7}$$

where, S_o is the location at which the value is to be predicted and $Z(S_o)$ is the value for the prediction location S_o, S_i is the i^{th} location and $Z(S_i)$ is the known value at the i^{th} location, λ_i is an unknown weight for the known value at the i^{th} location.

$$\lambda_i = \frac{d_i^{-p}}{\sum_{i=1}^{N} d_j^{-p}} \tag{8}$$

where, N is the total number of known points to be used for the interpolation technique, d is the distance of the unknown value location from the known value location, and p is a power parameter. The significance of the power parameter (p) is that its magnitude governs the assignments of weights to the points. A higher p value results in more weight being assigned to closer points, which means a less smooth gridded surface. On the other hand, a lower p value assigns relatively lower weights to closer points, which results into a much smoother surface. For the purpose of this study, the value of p was optimized using ArcGIS 10.2.

The aforementioned interpolation methodology was used to form gridded surfaces (rasters) of all the variables (precipitation, air temperatures, DTR, ET_o and AI). The point-based estimates of monthly summed precipitation amounts and monthly averages of maximum, minimum and mean air temperatures for each month of the 46 year study period were used as an input to the IDW interpolation tool in the Spatial Analyst Toolbox of ArcGIS 10.2. As a result, 552 rasters each of monthly summed precipitation, monthly averaged minimum, maximum and mean temperatures, DTR, monthly summed ET_o and monthly averaged AI were obtained. All these variables were rasterized for growing season and annual time steps. For analysis and inter-comparisons between different geographical areas, it was essential to compute

zone-based values from the continuous spatial datasets. For example, state or county-averaged magnitudes would enable interstate and intercounty comparison respectively. To extract these zonal values, zonal statistics tool in ArcGIS 10.2 was used.

RESULTS AND DISCUSSION

SPATIAL DISTRIBUTION OF AIR TEMPERATURES AND DAILY TEMPERATURE RANGE

The average maximum, minimum and mean air temperature (T_{max}, T_{min}, T_{mean}, respectively) and DTR from 1968 to 2013 were interpolated on a monthly, growing season and annual basis using the 800 weather stations in the study region (Figure 2). Tables 2, 3, 4 and 5 provide the statistics for monthly, growing season and annual T_{max}, T_{min}, T_{mean} and DTR on a statewide and regional average basis. Figures indicated that the study area has a north to south increasing trend, ranging from 6 to 30°C, when averaged annually; and ranged from 15 to 36°C, when averaged for the growing season. The regional average for T_{max} was 18.9°C on an annual basis and 28.6°C on a growing season basis. Also, the regional average T_{max} varied from 31.9°C in July to 5.2°C in January. Long-term monthly average maps for T_{max} are shown in Figure 3. Averaged annually, the lowest T_{max} was observed in the Cavalier county, North Dakota, while the highest was observed in Starr County, Texas. Averaged over the growing season, the lowest T_{max} was found in Lake County, Colorado, whereas the highest value was in Zapata County, Texas. Table 2 lists important statistics about statewide and regional T_{max}. On a monthly basis, the highest T_{max} values were observed in July and the lowest in January for all states as well as on a regional average basis. The seasonal behavior for T_{max} in all states was similar, with the highest values in JJA (June-July-August), followed by SON (September-October-November), MAM (March-April-May) and DJF (December-January-February). For the average annual T_{max}, the maximum standard deviation (SD) was observed in North Dakota (1.19^{o}C) and South Dakota (1.18^{o}C), while minimum values were in Oklahoma (0.70^{o}C) and Texas (0.67^{o}C). Generally, the SD decreased as we move north to south. For the growing season, the variation between the magnitudes of SD is not very high, with no discernible trend in the north-south direction. Also, for most of the states, the SD in growing season T_{max} is higher than those in annual T_{max}.

Minimum temperatures had a northwest-southeast increasing trend, ranging from -9 to 19°C when averaged annually; and from 0 to 25°C when averaged for the growing season (Figure 4). The long-term averaged monthly averaged maps for T_{avg} are shown in Figure 5. The regional average for the minimum temperature was 4.7°C on an annual basis and 13.8°C on a growing season basis. The regional average T_{min} ranged from 17.1°C in July to -8°C in January. Unlike annual averaged T_{max} where the lowest magnitudes were found in North Dakota, both the annual and growing season average lowest T_{min} values were observed in Lake County, Colorado. The highest magnitudes of both annual and growing season average T_{min} values were found in Cameron County, Texas. The SD in annual average T_{min} follows a decreasing trend in the north-south direction similar to T_{max}, but unlike growing season average T_{min}.

The regional scale magnitude of monthly averaged DTR varied from 13°C during December to 15.2°C during September. The annual and growing season averages for the region are 14.3°C and 14.8°C. Sun et al. (2006a) studied differences in season variations of DTR observed from surface and satellite observations and found that DTR obtained from surface air temperatures showed that DTR in summer is greater than in winter over the entire USA. Further, it can be observed from Figure 6 that the annual and growing season averaged DTR has a strong spatial variability, with the western part showing higher values of DTR, which gradually decreases as we move towards the east. Generally, the states of Colorado and Wyoming show the highest values of DTR in the region, while the lowest magnitudes were observed in Iowa. Also, high DTR magnitudes are found in the Rocky Mountains. It is also noteworthy that DTR values observed in the region is higher for the growing season than the annual values. The spatial distribution of DTR over the study region closely matches that of Sun et al. (2006b), who used satellite-based land surface temperature (LST) to evaluate DTR over the USA. Additional maps depicting the spatial distribution of monthly DTR over the study area are shown in Figure 7.

SPATIAL DISTRIBUTION OF PRECIPITATION

Daily precipitation data were summed to obtain monthly, growing season and annual precipitation from 1968 to 2013. This was followed by interpolation of the point-based values over the study region and averaging throughout the study period, which resulted in long-term average annual and growing season spatial precipitation maps (Figure 8). The descriptive statistics of monthly, annual and growing season precipitation for all states are presented in Table 6. In general, precipitation has a strong west to east increasing trend. Regionally, the annual and growing season precipitation varies from 163 to 1486 mm and from 98 to 746 mm, respectively. Averaged by state, the peak annual and growing season precipitation was observed in Oklahoma and Iowa, respectively, while the minimum values were observed in Wyoming. On a county basis, the maximum and minimum annual as well as growing season precipitation was observed in Orange County, Texas (1,459 mm) and Big Horn County, Wyoming (214 mm), respectively. The average regional annual and growing season precipitation amounts are 618 and 348 mm, respectively, which implies that the precipitation during the growing season months (May-September) contributes 56 % towards the annual precipitation. This contribution of growing season precipitation is highest in the state of South Dakota and Nebraska (65% each) and least in Texas (49%). The minimum SD in both annual and growing season precipitation was observed in Colorado and Wyoming and the highest in Iowa.

The timing of the peak precipitation amount varied with geographic location. The maximum precipitation in Nebraska, Kansas, Wyoming, Oklahoma and Texas occurred in May. In North Dakota, South Dakota and Iowa, the peak precipitation occurred in June, while in Colorado, it occurred in July. Both regionally and statewide, the minimum precipitation was observed in January. Sharma and Irmak (2012) showed the long-term (1986-2009) spatial distribution of precipitation for Nebraska and found similar results. Also, the annual precipitation spatial trends observed are concurrent with Kunkel et al. (2013), which relied on gridded COOP datasets to map annual average precipitation for the Great Plains. Wang et al. (2001) developed long- term (1989-1997) average annual precipitation map for Kansas,

which is coherent with our findings. To visualize the spatial patterns in monthly precipitation, spatial maps were generated for each month (Figure 9). These maps are instrumental in determining average monthly precipitation amounts in any geographical location in the region.

SPATIAL DISTRIBUTION OF REFERENCE EVAPOTRANSPIRATION

Daily ET_o estimates at point locations were used to compute monthly, growing season and annual estimates. These estimates were interpolated over the area and regional, state and county based values were extracted for comparison (Figure 10). The descriptive statistics for ET_o when averaged for statewide and regional basis are listed in Table 7. There is a strong southwest- northeast increasing trend in ET_o. The annual ET_o ranges from 824 mm in the Cavalier County, North Dakota to 2,590 mm in El Paso County, Texas. Similarly, the growing season ET_o ranges from 590 mm in the Allamakee County, Iowa to 1,427 mm in El Paso County, Texas. Considering statewide averages, both annual and growing season ET_o are highest in Texas and lowest in Iowa. The regional average annual and growing season ET_o values were 1,297 and 823 mm, respectively. Sharma and Irmak (2012) quantified and mapped alfalfa-reference ET (ET_r) in Nebraska, which are very similar to the maps of this study, when subset data for Nebraska are compared. Mutiibwa and Irmak (2013) mapped daily average ET_o computed from HS equation for June, July and August for 1982, 1990, 2002 and 2008 over the USA High Plains. The spatial distribution of these maps was similar to our monthly averaged maps, although our maps represent monthly summed ET_o, rather than daily average ET_o. Also, ET_o quantification in our study involved vigorous spatial and temporal calibration of HS equation using site-specific, month-specific calibration coefficients, while Mutiibwa and Irmak (2013) used the original form of HS equation. Borrelli et al. (1998) mapped long-term (30-year) annual average ET_o for Texas and found similar trends across the state as this study.

The maximum monthly ET_o was observed in July in all states while both January and December had minimum ET_o. The contribution of growing season towards annual ET_o was 63%, averaged regionally. This contribution was maximum for North Dakota (73%) and minimum for Texas (57%).

Generally, the magnitude of this contribution decreased when moving north to south. The seasonal behavior in ET_o is very consistent for all states, with the highest ET_o occurring in JJA, followed by MAM, SON and DJF. The SD for annual ET_o is greater than that of growing season ET_o for all states. For both annual and growing season ET_o, the highest SD is observed in South Dakota and the least in Colorado. For more details, the maps showing the spatial distribution of ET_o averaged for each month of the year are shown in Figure 11.

SPATIAL DISTRIBUTION OF ARIDITY INDEX

The he magnitude of AI (Figure 12) increases when moving from west to east, which indicates that the climate becomes more humid or less arid as moving east. Higher values of AI are observed where the precipitation amount is much higher than the ET_o at a particular location, and lower values where the precipitation is less than the ET_o. Table 8 lists the descriptive statistics for AI averaged on statewide and regional basis. Regional average annual and growing season ET_o is 0.49 and 0.44, respectively, which falls into the semi-arid class. This does not necessarily mean that the region is dominantly semi-arid, since there is a high degree of spatial variation observed in the AI values in the region. Figure 13 represents the aridity classes that were delineated for the region based on the annual AI. For example, the average AI calculated in Iowa is the highest among all the states for all months, annually as well as for the growing season. The AI in Iowa ranged from 2.21 in December to 0.74 in July, implying that the state lies in the humid class. The lowest magnitudes of AI were observed in Wyoming and Colorado, with annual and growing season AI, respectively, of 0.27 and 0.22 for Wyoming; and 0.29 and 0.25 for Colorado respectively, meaning that the region lies in the semi-arid class. In terms of monthly AI magnitudes, the highest values were observed in December and January and lowest during June-July. This is explained by the monthly distribution of both precipitation and ET_o. Although the seasonal trends in precipitation and ET_o amounts are similar (highest in summers and lowest in winters), the rates of increase and decrease are differential, which results in the magnitudes of summer ET_o being much higher than that of summer precipitation. However, this difference narrows towards the winter season, resulting in higher ratios of

monthly precipitation to ET_o, or AI. The highest magnitude of SD in annual and growing season AI was observed in Iowa, and the least was observed in Colorado and Wyoming. Sankarasubramanian and Vogel (2003) developed spatial maps of hydroclimatological indices for the US, AI and observed spatial distribution closely related to the findings of our study, where the AI magnitudes increase when moving eastwards. Due to variation in monthly distribution of the two drivers of the AI, i.e., precipitation and ET_o, it is expected that consequently, considerable variation would occur in monthly AI magnitudes over the region. To visualize this variation, detailed maps depicting monthly AI were developed (Figure 14).

SUMMARY AND CONCLUSIONS

The objective this study was to quantify, map and analyze large-scale and long-term air temperatures, DTR, precipitation, ET_o and AI from 1968 to 2013 over the Great Plains of USA. Point-based weather data from over 800 stations was used to estimate all of the aforementioned variables, and subsequently to interpolate the same using Inverse Distance Weighing technique. An AI [adopted from UNEP (1997)] was quantified using the spatial datasets of precipitation and ET_o. Long-term average maps for all individual months and growing season and annual basis were developed to be used for spatial analyses. Long-term annual average air temperatures (T_{max}, T_{min}, T_{avg}) followed strong north-south increasing trends throughout the region, with exceptionally lower temperatures observed in the Rocky Mountain ranges. Similar spatial behavior was observed for long-term average growing season monthly average air temperatures. DTR at all three temporal scales (monthly, annual and growing season) showed decreasing trends as moving from west to east. On the contrary, precipitation exhibited increasing trends from west to east on all temporal scales. ET_o displayed strong spatial patterns over the study region, decreasing in a southwest to northeast direction. AI, as a result of magnitudes of both precipitation and ET_o, showed a gradual increase (more humid) towards east. According to the UNEP classification, the study area can be divided into arid, semi-arid, dry sub humid and humid regions based on AI magnitudes. For all of the aforementioned variables, regional, statewide and countywide values were extracted and analyzed.

Extensive maps and spatiotemporal datasets developed, presented and analyzed in this study have the potential to provide invaluable data and information to environmental/meteorological and water management personnel, water resources scientists and researchers as well as policy and decision making agencies for large scale assessments of climate and water resources interactions. Due to consideration of multiple spatial units, such as states and counties, the information is quite appropriate for a range of applications. Combined analyses of spatial distribution of precipitation and ET_o, which are important drivers of various processes in hydrologic cycle, can provide insightful background for climate change studies in the region. The variables quantified on a growing season basis can aid in observing all the relevant factors, specifically for the agricultural and natural resources applications. For example, growing season ET_o indicates the atmospheric evaporative demand for actual crop ET, due to which it can be used as an estimate for upper limit of water loss from an agricultural area. Identification of priority areas and their evaluation in terms of water supply and demand can be carried out using maps developed in this research. Successively, these maps can lead to take proactive actions to establish a balance between water supply and demand and forecasting these balances. These actions can include modification of the cropping patterns towards lower water demand cropping systems, adoption of reduced tillage practices to minimize soil evaporation, implementation of drought-tolerant crop hybrids and implementation of deficit irrigation strategies. Part II of this research [Kukal and Irmak (2016)] builds upon the monthly, growing season and annual datasets of all the variables discussed in the Part I from 1968 to 2013 and uses GIS tools to extract county-scale values of the variables in order to construct a time series for the research period, which were then subjected to temporal trend tests to investigate and analyze long-term trends in the region.

ACKNOWLEDGEMENT

This study is based upon the work that is supported by the National Institute of Food and Agriculture, U.S. Department of Agriculture, Hatch Project, under the Project Number NEB-21-167. This study was supported by the grants from the Nebraska Environmental Trust (NET) under the project

agreement #13-146 and the Central Platte Natural Resources District (CPNRD) under the grant agreement #38484. The projects Principal Investigator, Dr. Suat Irmak, expresses his appreciation to USDA-NIFA, NET and CPNRD.

REFERENCES

Borrelli, J., 1998. Mean crop consumptive use and free-water evaporation for Texas, Department of Civil Engineering, Texas Tech University.

Courault, D., Monestiez, P., 1999. Spatial interpolation of air temperature according to atmospheric circulation patterns in southeast France. Int. J. Climatol. 19, 365-378.

Dodson, R., Marks, D., 1997. Daily air temperature interpolated at high spatial resolution over a large mountainous region. Climate Research. 8, 1-20.

Doorenbos, J., Pruitt, W., 1977. Crop water requirements. FAO irrigation and drainage paper 24. Land and Water Development Division, FAO, Rome, 144 pp.

Hargreaves, G.H., Samani, Z.A., 1985. Reference crop evapotranspiration from ambient air temperature. American Society of Agricultural Engineers (Microfiche collection)(USA).no.fiche no.85-2517.

Holdaway, M.R., 1996. Spatial modeling and interpolation of monthly temperature using kriging. Climate Research. 6, 215-225.

Hulme, M., Conway, D., Jones, P., Jiang, T., Barrow, E., Turney, C., 1995. Construction of a 1961-1990 European climatology for climate change modelling and impact applications. Int.J.Climatol. 15, 1333-1364.

Hulme, M., Conway, D., Joyce, A., Mulenga, H., 1996. A 1961-90 climatology for Africa south of the equator and a comparison of potential evapotranspiration estimates. S. Afr.J.Sci. 92, 334-343.

Irmak, S., 2010. Nebraska water and energy flux measurement, modeling, and research network (NEBFLUX). Transactions of the ASABE. 53, 1097-1115.

Irmak, S., Kabenge, I., Skaggs, K.E., Mutiibwa, D., 2012. Trend and magnitude of changes in climate variables and reference evapotranspiration over 116-yr period in the Platte River Basin, central Nebraska–USA. Journal of Hydrology. 420, 228-244.

Kukal, M., Irmak, S., 2016. Long-Term Patterns of Air Temperatures, Daily Temperature Range, Precipitation, Grass-Reference Evapotranspiration and Aridity Index in The USA Great Plains: Part II. Temporal Trends. Journal of Hydrology.

Kukal, M., Irmak S., Odhiambo, L.O., Walia, H., 2016. Spatial and Temporal Performance, Calibration and Validation of Hargreaves-Samani Equation for Quantification of Grass-Reference Evapotranspiration in The USA Great Plains. Journal of Irrigation and Drainage Engineering (Submitted).

Kunkel, K.E., 2013. Regional Climate Trends and Scenarios for the U.S. National Climate Assessment. Part 4. Climate of the U.S. Great Plains. NOAA Technical Report NESDIS 142-4.

Kurtzman, D., Kadmon, R., 1999. Mapping of temperature variables in Israel: a comparison of different interpolation methods. Climate Research. 13, 33-43.

Mannocchi, F., Todisco, F., Vergni, L., 2005. 58. Agricultural Drought: Indices, Definition and Analysis. Water and Energy Abstracts. 15, 21-21.

Mather, J.R., Bullock, A., Woodings, R.B., 1978. The climatic water budget in environmental analysis, Lexington Books Lexington, MA.

McCloud, D., 1955. Water requirements of field crops in Florida as influenced by climate. Proc.Soil Sci.Soc.Fla. 15, 165-172.

McGuinness, J.L., Bordne, E.F., 1972. A comparison of lysimeter-derived potential evapotranspiration with computed values, US Dept. of Agriculture.

Monteith, J. L., 1965. Evaporation and environment. In Symp. Soc. Exp. Biol. 19 (205-23) 4.

Mutiibwa, D., Irmak, S., 2013. AVHRR-NDVI-based crop coefficients for analyzing long-term trends in evapotranspiration in relation to changing climate in the US High Plains. Water Resour.Res. 49, 231-244.

Ninyerola, M., Pons, X., Roure, J.M., 2007. Monthly precipitation mapping of the Iberian Peninsula using spatial interpolation tools implemented in a Geographic Information System. Theoretical and Applied Climatology. 89, 195-209.

Penman, H.l. 1948. Natural evaporation from open water, hare soil and grass. Proc.R.Soc.Lond.A.Math.Phys.Sci. 193, 120-145.

Rosenberg, N.J., Epstein, D.J., Wang, D., Vail, L., Srinivasan, R., Arnold, J.G., 1999. Possible impacts of global warming on the hydrology of the Ogallala aquifer region. Clim.Change. 42, 677-692.

Rossum, S., Lavin, S., 2000. Where are the Great Plains? A cartographic analysis. The Professional Geographer. 52, 543-552.

Sankarasubramanian, A., Vogel, R.M., 2003. Hydroclimatology of the continental United States. Geophys.Res.Lett. 30.

Sharma, V., Irmak, S., 2012. Mapping spatially interpolated precipitation, reference evapotranspiration, actual crop evapotranspiration, and net irrigation requirements in Nebraska: part I. Precipitation and Reference evapotranspiration. Transactions of the ASABE, 55(3), 907-921

Skaggs, K.E., Irmak, S., 2012. Long-term trends in air temperature distribution and extremes, growing degree-days, and spring and fall frosts for climate impact assessments on agricultural practices in nebraska. Journal of Applied Meteorology and Climatology. 51, 2060-2073.

Sun, D., Pinker, R.T., Kafatos, M., 2006. Diurnal temperature range over the United States: A satellite view. Geophys.Res.Lett. 33.

Sun, D., Kafatos, M., Pinker, R.T., Easterling, D.R., 2006. Season variations in diurnal temperature range from satellites and surface observations. Geoscience and Remote Sensing, IEEE Transactions on. 44, 2779-2785.

Turc, L., 1961. Estimation of irrigation water requirements, potential evapotranspiration: a simple climatic formula evolved up to date. Ann.Agron. 12, 13-49.

UNEP (United Nations Environment Programme), 1997. World atlas of desertification 2ED. UNEP, London.

United Nations Educational, Scientific and Cultural Organization (UNESCO), 1979. Map of the world distribution of arid regions: Map at scale 1:25,000,000 with explanatory note. MAB Technical Notes 7, UNESCO, Paris.

Wang, J., Price, K., Rich, P., 2001. Spatial patterns of NDVI in response to precipitation and temperature in the central Great Plains. Int.J.Remote Sens. 22, 3827-3844.

Willmott, C.J., Matsuura, K., 1995. Smart interpolation of annually averaged air temperature in the United States. J.Appl.Meteorol. 34, 2577-2586.

Willmott, C.J., Robeson, S.M., 1995. Climatologically aided interpolation (CAI) of terrestrial air temperature. Int.J.Climatol. 15, 221-230.

Table 1. Climate classification based on Aridity Index

Climate Class	Aridity Index
Hyper-arid	<0.03
Arid	0.03 – 0.20
Semi-arid	0.20 – 0.50
Dry sub humid	0.50 – 0.65
Humid	>0.65

Table 2. Regional and statewide statistics for monthly, growing season and annual maximum air temperature (°C).

Months	Regional	ND	SD	NE	KS	CO	WY	IA	OK	TX
Monthly means										
January	5.2	-7.2	-2.2	1.9	5.3	3.6	0.2	-2.3	9.4	14.7
February	7.9	-3.8	0.8	4.8	8.2	6.0	2.6	0.8	12.2	17.0
March	13.2	2.8	6.9	10.5	14.0	10.7	7.8	7.9	17.4	21.4
April	19.1	12.5	14.8	16.9	19.8	15.5	13.0	16.1	22.7	25.8
May	24.1	19.7	21.1	22.5	24.7	20.9	18.6	22.2	26.8	29.5
June	29.1	24.6	26.4	28.2	30.4	26.9	24.6	27.3	31.6	33.1
July	31.9	28.2	30.5	31.4	33.5	29.9	29.5	29.5	34.6	34.5
August	31.2	27.7	29.7	30.4	32.5	28.5	28.5	28.3	34.3	34.4
September	26.7	21.7	24.4	25.7	27.8	24.2	22.7	24.2	29.6	31.0
October	20.2	13.4	16.1	18.4	21.0	17.5	15.0	17.2	23.5	26.1
November	12.3	3.1	6.6	9.6	12.9	9.7	6.4	8.1	16.3	20.1
December	6.4	-4.7	-0.5	3.2	6.6	4.1	0.7	0.0	10.6	15.6
Annual										
Mean	18.9	11.5	14.6	17	19.7	16.5	14.1	14.9	22.4	25.3
Max	21.0	14.0	17.2	19.7	22.2	18.4	16.3	17.6	24.4	27.0
Min	17.4	9.0	11.9	14.5	17.5	15.0	12.0	12.9	21.2	24.2
SD	0.7	1.2	1.2	1.0	0.9	0.7	0.8	1.0	0.7	0.7
Growing Season										
Mean	28.6	24.4	26.4	27.6	29.8	26.1	24.8	26.3	31.4	32.5
Max	30.4	27.3	28.9	30.3	32.1	28.1	27.1	29.4	33.9	35.5
Min	27.1	21.6	23.3	25.3	27.6	24.5	22.4	24.1	29.1	31.0
SD	0.7	1.1	1.2	1.0	1.0	0.8	1.0	1.0	1.1	0.9

Table 3. Regional and statewide statistics for monthly, growing season and annual minimum air temperature (°C).

Months	Regional	ND	SD	NE	KS	CO	WY	IA	OK	TX
Monthly means										
January	-8.0	-18.2	-14.1	-11.2	-7.9	-12.0	-12.9	-12.6	-3.7	0.7
February	-5.7	-15.0	-11.3	-8.7	-5.6	-9.9	-11.1	-9.8	-1.5	2.6
March	-0.9	-8.6	-5.8	-3.8	-0.6	-5.5	-6.4	-3.4	3.2	6.6
April	4.3	-1.0	0.6	1.9	5.0	-1.1	-2.1	3.1	8.3	11.0
May	9.7	5.6	6.8	8.0	10.8	3.9	2.8	9.4	13.6	15.8
June	14.5	11.0	12.2	13.5	16.3	8.6	7.5	14.8	18.6	19.8
July	17.1	13.7	15.5	16.6	19.2	11.9	10.9	17.3	21.0	21.3
August	16.2	12.5	14.2	15.4	18.2	11.0	9.8	15.9	20.3	20.9
September	11.5	6.8	8.5	9.7	12.9	6.3	4.5	10.8	15.8	17.5
October	5.2	0.1	1.7	2.7	6.0	0.0	-1.1	4.2	9.2	11.8
November	-1.2	-7.7	-5.6	-4.2	-0.8	-6.1	-7.1	-2.5	2.9	5.9
December	-6.5	-15.2	-12.0	-9.7	-6.2	-11.0	-12.1	-9.6	-2.3	1.6
Annual										
Mean	4.7	-1.3	0.9	2.5	5.6	-0.3	-1.4	3.1	8.8	11.3
Max	6.0	1.2	2.6	3.9	6.9	0.9	0.0	5.2	10.1	12.5
Min	3.5	-3.3	-0.7	1.2	4.4	-1.4	-2.9	1.7	7.6	9.9
SD	0.6	1.0	0.9	0.7	0.6	0.6	0.7	0.8	0.5	0.6
Growing Season										
Mean	13.8	9.9	11.5	12.7	15.5	8.4	7.1	13.6	17.9	19.0
Max	15.0	11.5	13.0	14.0	16.7	9.5	8.8	15.0	19.5	20.6
Min	12.8	8.4	9.9	11.3	14.2	7.1	5.8	12.0	16.3	17.5
SD	0.5	0.8	0.7	0.6	0.6	0.6	0.7	0.7	0.7	0.7

Table 4. Regional and statewide statistics for monthly, growing season and annual mean air temperature (°C).

Months	Regional	ND	SD	NE	KS	CO	WY	IA	OK	TX
Monthly means										
January	-1.4	-12.7	-8.1	-4.6	-1.3	-4.2	-6.4	-7.4	2.8	7.7
February	1.1	-9.4	-5.2	-2.0	1.3	-1.9	-4.3	-4.5	5.3	9.8
March	6.1	-2.9	0.6	3.4	6.7	2.6	0.7	2.3	10.3	14.0
April	11.7	5.8	7.7	9.4	12.4	7.2	5.5	9.6	15.5	18.4
May	16.9	12.7	13.9	15.2	17.7	12.4	10.7	15.8	20.2	22.6
June	21.8	17.8	19.3	20.9	23.3	17.7	16.0	21.1	25.1	26.4
July	24.5	21.0	23.0	24.0	26.3	20.9	20.2	23.4	27.8	27.9
August	23.7	20.1	22.0	22.9	25.3	19.8	19.2	22.1	27.3	27.7
September	19.1	14.3	16.5	17.6	20.3	15.3	13.6	17.5	22.7	24.2
October	12.7	6.7	8.9	10.5	13.5	8.8	6.9	10.7	16.4	19.0
November	5.5	-2.3	0.5	2.7	6.0	1.8	-0.4	2.8	9.6	13.0
December	-0.1	-10.0	-6.3	-3.2	0.2	-3.5	-5.7	-4.8	4.2	8.6
Annual										
Mean	11.8	5.1	7.7	9.7	12.7	8.1	6.3	9.0	15.6	18.3
Max	13.4	7.6	9.7	11.5	14.4	9.6	8.2	11.0	17.0	19.6
Min	10.7	2.9	5.6	8.1	11.2	7.0	4.6	7.4	14.5	17.2
SD	0.6	1.1	1.0	0.8	0.7	0.6	0.7	0.8	0.5	0.6
Growing Season										
Mean	21.2	17.2	18.9	20.1	22.6	17.2	15.9	20.0	24.6	25.8
Max	22.4	19.4	20.8	21.6	24.3	18.8	17.7	22.0	26.6	27.8
Min	12.8	8.4	9.9	11.3	14.2	7.5	5.9	12.0	16.7	18.3
SD	3.0	3.0	3.2	3.1	3.0	3.7	3.6	2.7	2.8	2.7

Table 5. Regional and statewide statistics for monthly, growing season and annual average daily temperature range (DTR) (°C)

Months	Regional	ND	SD	NE	KS	CO	WY	IA	OK	TX
Monthly mean										
January	13.2	11.0	11.9	13.1	13.1	15.6	13.1	10.3	13.1	13.9
February	13.6	11.2	12.1	13.5	13.8	15.9	13.7	10.5	13.7	14.4
March	14.1	11.4	12.7	14.3	14.6	16.1	14.2	11.3	14.1	14.8
April	14.8	13.5	14.2	15.0	14.8	16.6	15.1	13.0	14.4	14.8
May	14.4	14.2	14.3	14.4	13.9	16.9	15.8	12.8	13.2	13.7
June	14.5	13.6	14.2	14.7	14.1	18.4	17.2	12.5	13.0	13.3
July	14.8	14.5	15.0	14.8	14.4	18.0	18.5	12.2	13.6	13.2
August	15.0	15.3	15.5	14.9	14.3	17.5	18.7	12.3	13.9	13.6
September	15.2	14.9	15.8	16.0	14.8	18.0	18.2	13.4	13.8	13.5
October	14.9	13.3	14.5	15.7	15.1	17.5	16.1	13.0	14.4	14.3
November	13.5	10.8	12.1	13.8	13.8	15.7	13.5	10.6	13.4	14.2
December	13.0	10.5	11.5	13.0	12.8	15.2	12.9	9.6	12.9	14.0
Annual										
Mean	14.3	12.9	13.6	14.4	14.1	16.8	15.6	11.8	13.6	14.0
Max	15.4	14.7	15.5	16.5	15.7	17.8	16.6	13.7	15.0	15.3
Min	13.4	11.7	12.3	12.8	12.6	15.8	14.5	10.1	12.6	12.7
SD	0.5	0.7	0.8	0.7	0.7	0.5	0.5	0.7	0.6	0.5
CV	3.3	5.1	5.6	4.9	4.7	2.7	3.3	5.8	4.2	3.9
Growing Season										
Mean	14.8	14.5	15.0	15.0	14.3	17.7	17.7	12.6	13.5	13.5
Max	15.9	16.7	17.4	17.5	16.3	19.2	19.3	14.8	15.1	15.3
Min	13.9	12.7	13.2	13.0	12.9	16.6	16.2	10.6	11.6	11.8
SD	0.5	0.8	1.0	0.9	0.8	0.6	0.7	0.8	0.7	0.5
CV	3.6	5.7	6.5	5.7	5.4	3.2	4.0	6.6	5.4	4.0

Table 6. Regional and statewide statistics for monthly, growing season and annual average precipitation (mm)

Months	Regional	ND	SD	NE	KS	CO	WY	IA	OK	TX
Monthly mean										
January	26	14	13	13	18	18	14	25	37	43
February	28	12	16	16	25	18	15	27	44	43
March	42	23	32	38	54	28	21	54	75	51
April	55	38	57	63	67	35	34	89	82	53
May	81	66	79	93	102	43	51	113	121	85
June	79	84	85	89	99	36	40	120	106	83
July	65	68	67	78	88	50	30	106	70	62
August	61	53	54	68	83	49	25	104	73	64
September	61	44	45	53	66	35	27	85	89	82
October	55	37	44	46	58	30	27	67	84	75
November	35	18	20	25	37	21	18	49	61	50
December	29	15	14	16	26	19	16	34	47	45
Annual										
Mean	618	472	523	598	724	380	317	874	888	737
Max	752	617	662	836	1029	474	450	1220	1179	1027
Min	466	299	338	346	504	245	194	557	644	386
SD	70	76	87	103	111	52	52	140	130	125
CV	11	16	17	17	15	14	17	16	15	17
Growing Season										
Mean	348	322	343	392	444	218	175	534	463	364
Max	445	458	466	600	708	290	258	914	700	570
Min	238	192	208	167	249	133	83	300	273	138
SD	47	62	61	76	97	36	37	111	99	76
CV	14	19	18	19	22	16	21	21	21	21

Table 7. Regional and statewide statistics for monthly, growing season and annual ET_o (mm).

Months	Regional	ND	SD	NE	KS	CO	WY	IA	OK	TX
Monthly mean										
January	39	8	19	31	39	41	26	17	49	67
February	49	14	27	39	49	49	33	24	60	81
March	83	42	60	75	84	84	68	54	96	117
April	120	96	105	114	120	116	100	99	131	148
May	153	140	147	148	148	151	139	133	154	173
June	179	153	168	174	179	190	177	147	183	196
July	190	173	192	186	193	198	193	148	202	199
August	172	155	169	162	170	173	172	125	184	189
September	129	109	125	127	132	134	120	98	136	144
October	90	66	78	86	93	95	75	68	97	111
November	54	29	39	48	54	56	40	36	61	78
December	39	12	21	31	37	40	25	18	46	65
Annual										
Mean	1297	996	1149	1223	1298	1327	1169	966	1399	1569
Max	1411	1123	1287	1390	1443	1449	1290	1092	1507	1718
Min	1212	907	1022	1091	1176	1247	1056	846	1319	1479
SD	35	50	59	52	46	38	43	45	43	44
CV	3	5	5	4	4	3	4	5	3	3
Growing Season										
Mean	823	731	800	799	822	846	801	650	859	902
Max	881	823	885	894	906	906	864	743	942	1010
Min	773	648	704	723	753	794	727	577	787	825
SD	24	33	39	35	35	24	29	30	35	30
CV	3	5	5	4	4	3	4	5	4	3

Table 8. Regional and statewide statistics for monthly, growing season and annual Aridity Index.

Months	Regional	ND	SD	NE	KS	CO	WY	IA	OK	TX
Monthly mean										
January	0.85	0.87	1.49	0.50	0.55	0.54	0.81	2.00	0.83	0.76
February	0.68	0.97	0.77	0.50	0.59	0.45	0.52	1.30	0.82	0.63
March	0.56	0.65	0.58	0.55	0.69	0.36	0.33	1.06	0.82	0.49
April	0.49	0.44	0.57	0.58	0.59	0.32	0.36	0.93	0.65	0.41
May	0.56	0.49	0.56	0.65	0.73	0.30	0.38	0.88	0.82	0.54
June	0.47	0.56	0.52	0.53	0.59	0.20	0.23	0.84	0.61	0.46
July	0.37	0.41	0.37	0.43	0.48	0.26	0.16	0.74	0.37	0.34
August	0.38	0.35	0.33	0.44	0.51	0.29	0.15	0.85	0.41	0.35
September	0.50	0.43	0.39	0.44	0.55	0.27	0.24	0.90	0.70	0.60
October	0.64	0.61	0.60	0.56	0.68	0.34	0.38	1.01	0.95	0.74
November	0.73	0.75	0.60	0.58	0.76	0.42	0.50	1.50	1.12	0.73
December	0.95	1.90	0.80	0.61	0.78	0.58	0.78	2.21	1.12	0.80
Annual										
Mean	0.49	0.48	0.46	0.50	0.58	0.29	0.27	0.91	0.66	0.50
Max	0.63	0.67	0.65	0.78	0.87	0.38	0.41	1.45	0.91	0.72
Min	0.34	0.27	0.27	0.25	0.36	0.17	0.15	0.52	0.45	0.24
SD	0.07	0.09	0.09	0.10	0.11	0.05	0.05	0.18	0.11	0.09
CV	13.32	19.30	20.60	20.41	18.42	15.64	19.46	19.36	16.92	19.04
Growing Season										
Mean	0.44	0.44	0.42	0.49	0.56	0.25	0.22	0.82	0.55	0.44
Max	0.6	0.71	0.67	0.84	0.97	0.36	0.34	1.59	0.91	0.72
Min	0.3	0.24	0.24	0.19	0.28	0.15	0.10	0.42	0.31	0.15
SD	0.1	0.10	0.10	0.11	0.14	0.05	0.05	0.20	0.14	0.10
CV	15.99	23.02	22.72	23.45	25.71	18.94	24.27	24.25	25.06	22.61

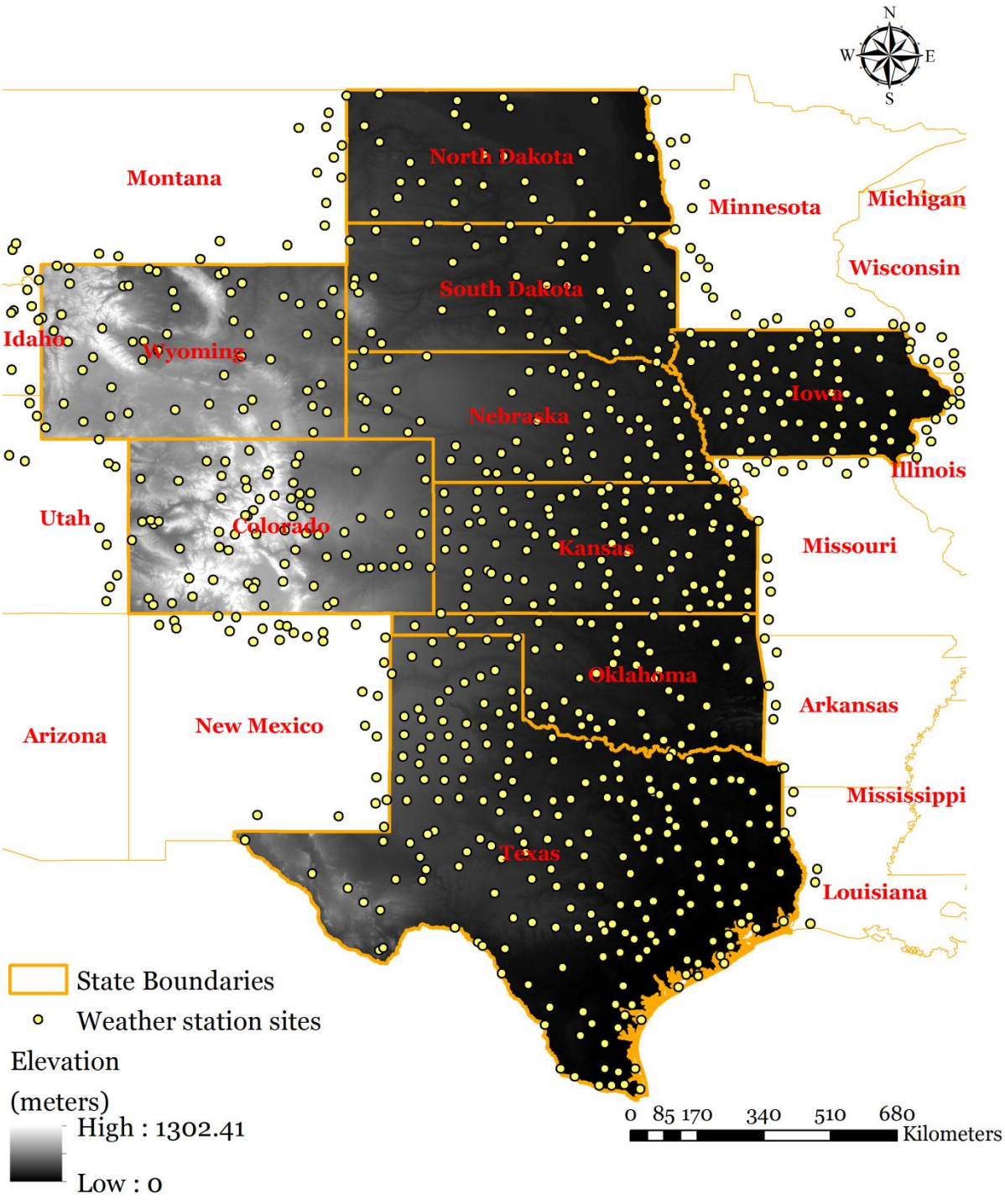

Figure 1. Map of study area and geographical locations of the weather station sites used in the interpolation process of the variables.

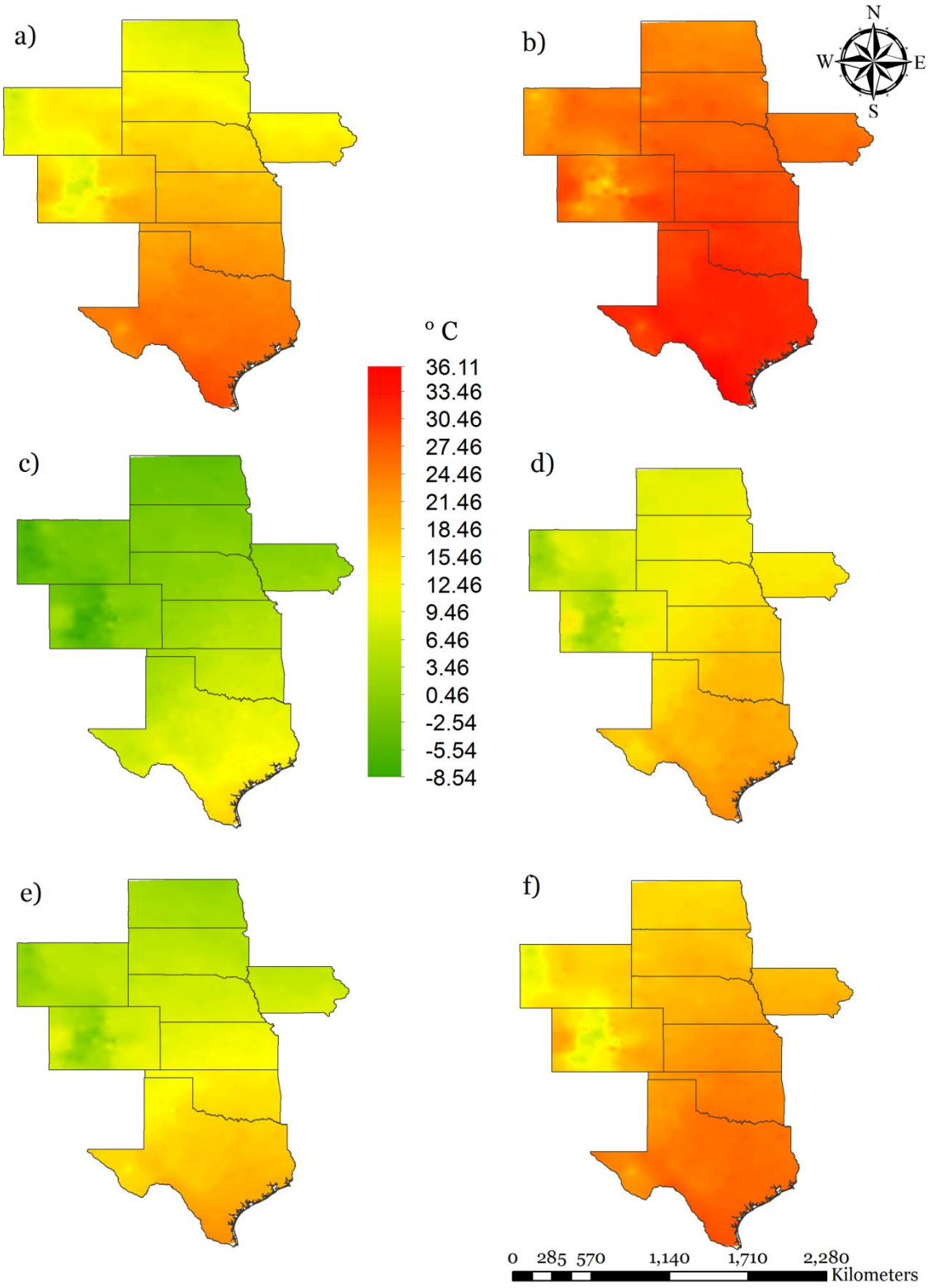

Figure 2. Spatial distribution of average a) annual T_{max}, b) growing season T_{max}, c) annual T_{min}, d) growing season T_{min}, e) annual T_{avg}, f) growing season T_{avg}.

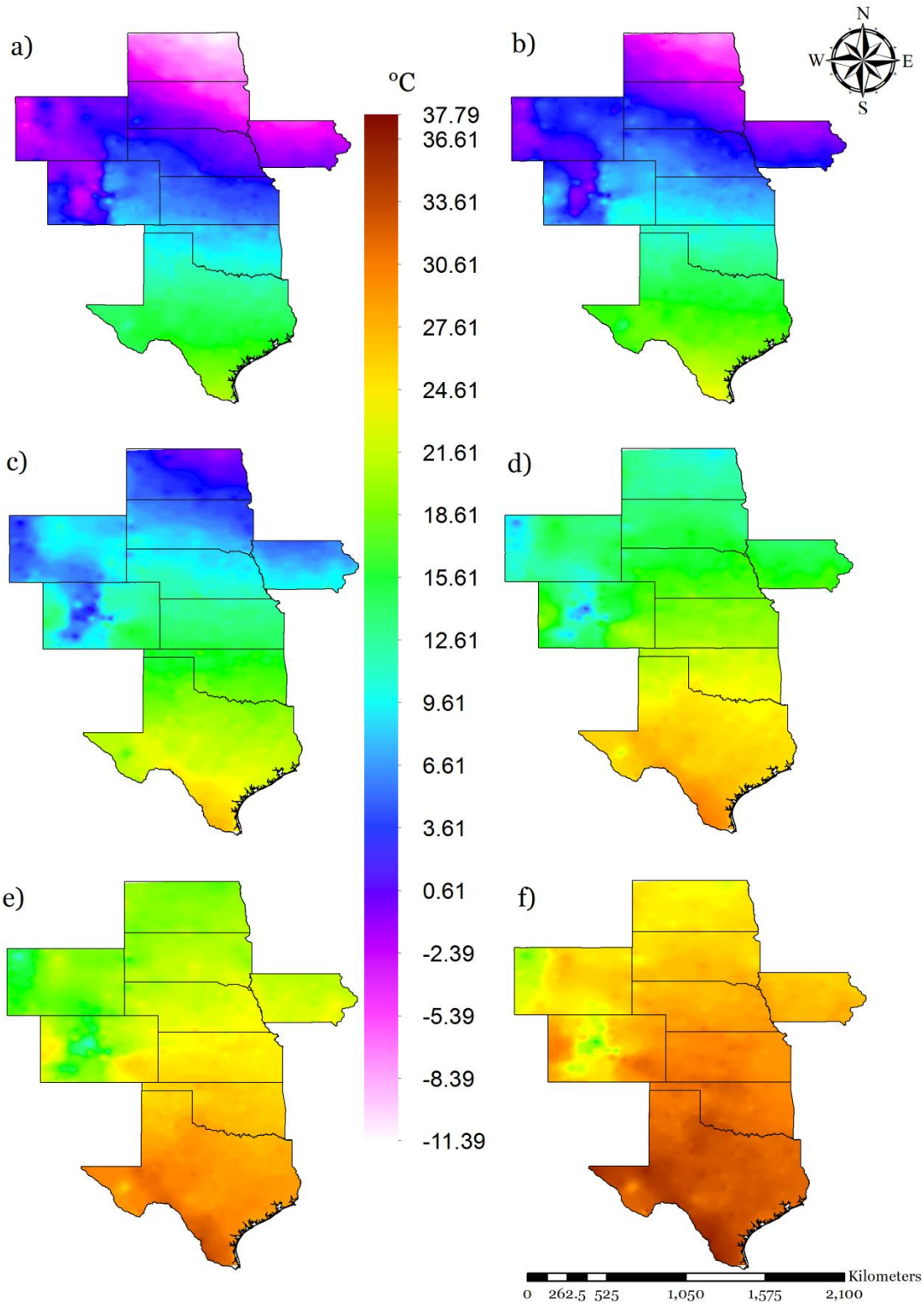

Figure 3. Spatial distribution of long-term average monthly maximum air temperature for a) January, b) February, c) March, d) April, e) May, f) June, g) July, h) August, i) September, j) October, k) November and l) December.

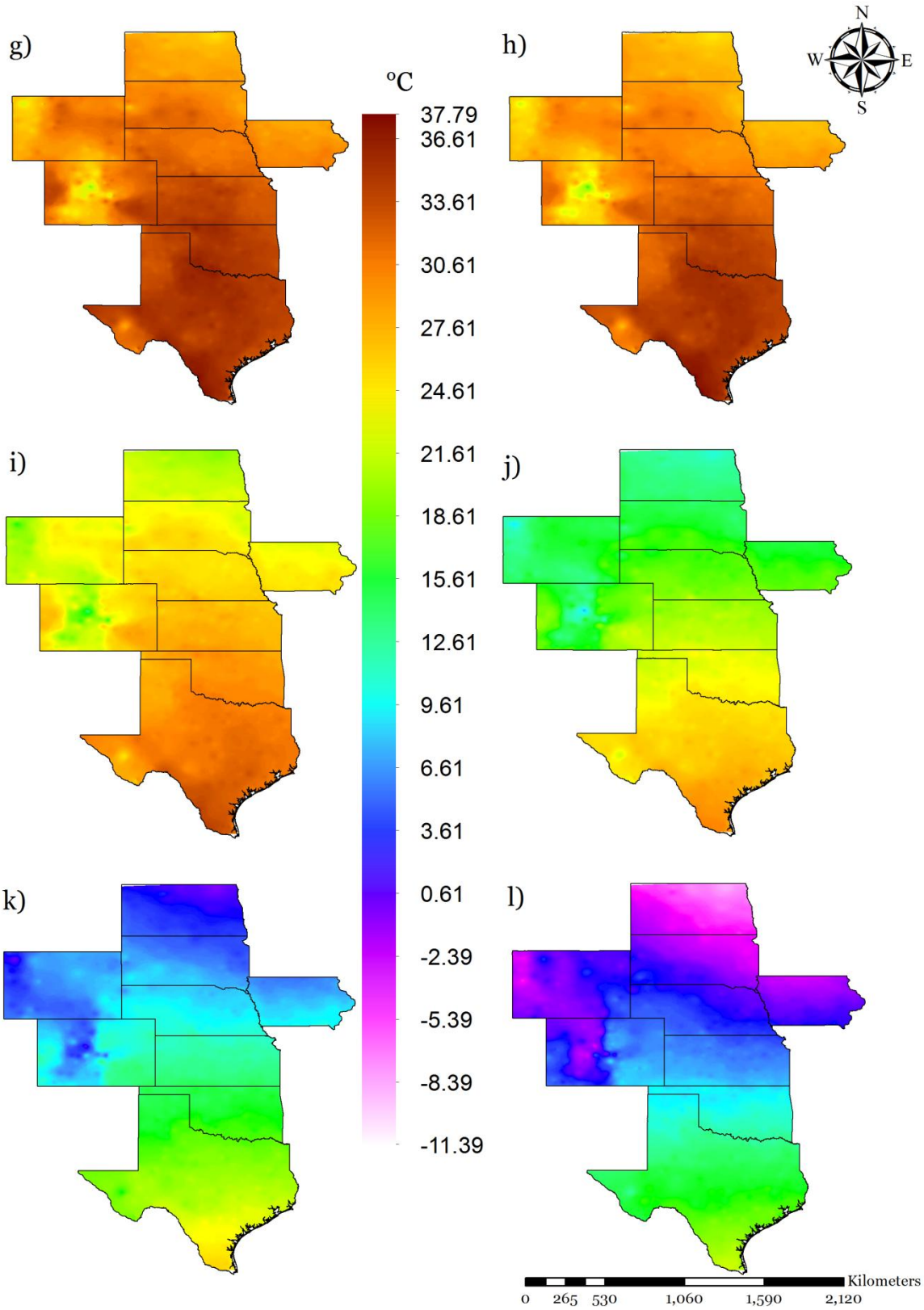

Figure 3 (cont.). Spatial distribution of long-term average monthly maximum air temperature for a) January, b) February, c) March, d) April, e) May, f) June, g) July, h) August, i) September, j) October, k) November and l) December.

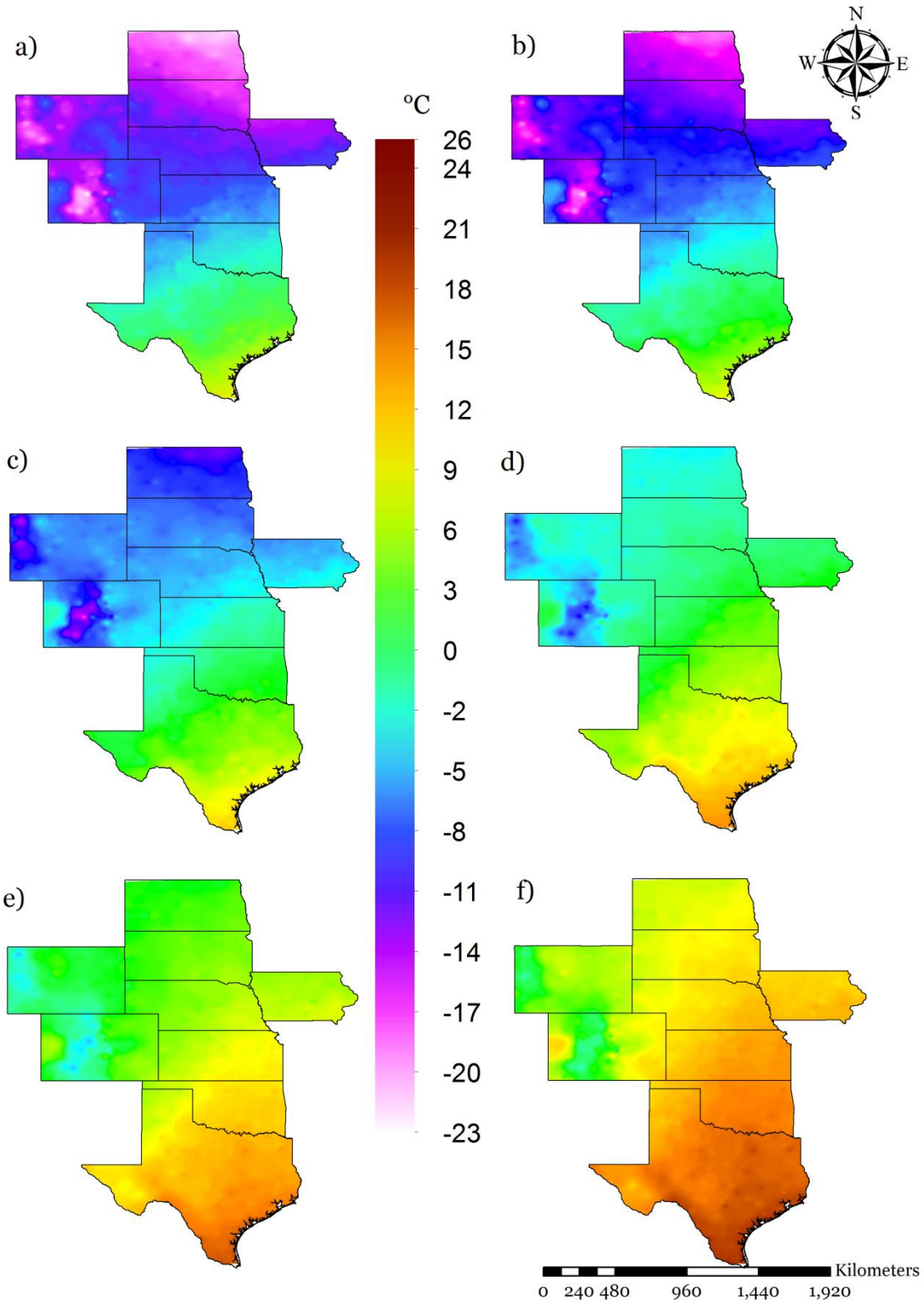

Figure 4. Spatial distribution of long-term average monthly minimum air temperature for a) January, b) February, c) March, d) April, e) May, f) June, g) July, h) August, i) September, j) October, k) November and l) December.

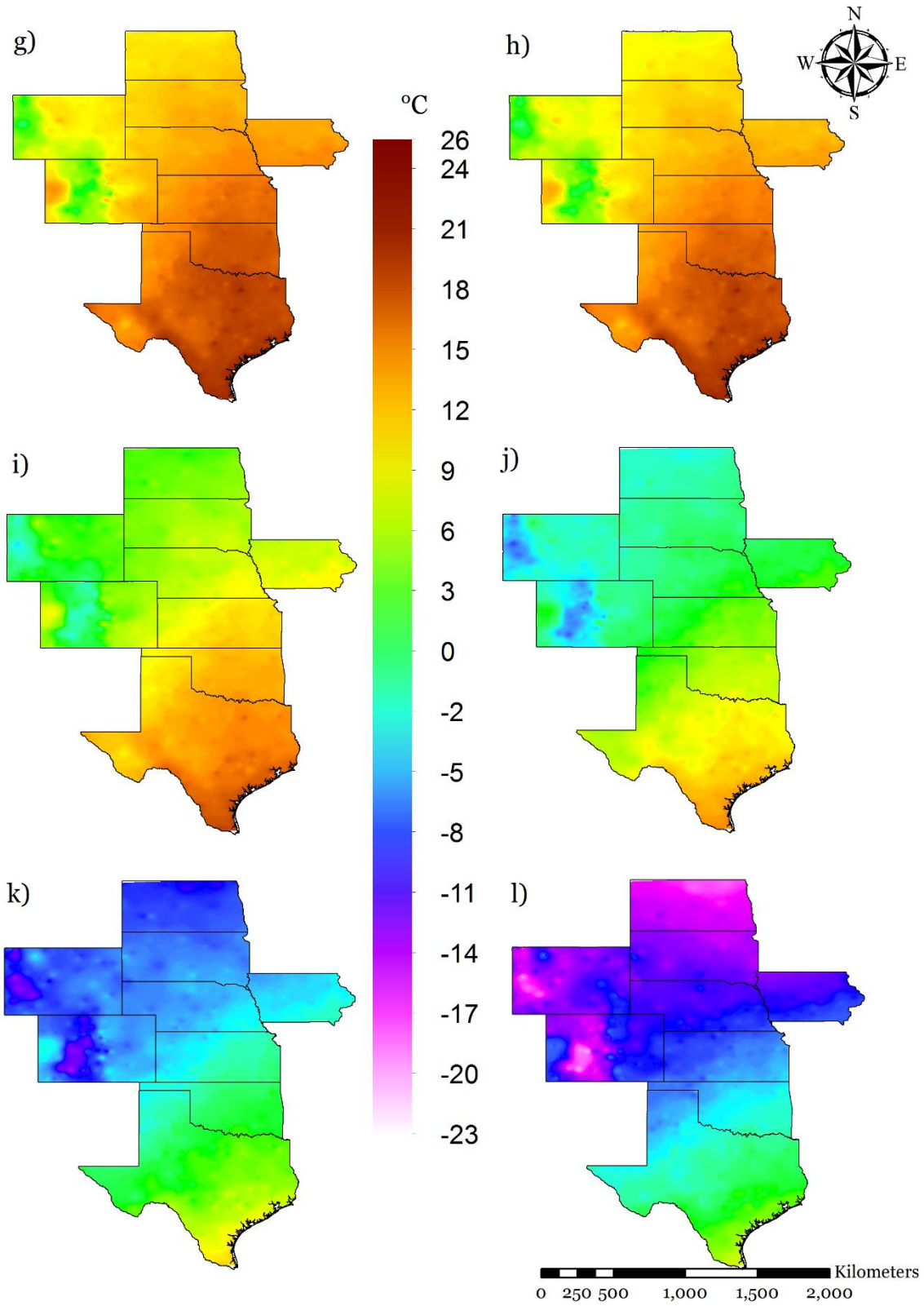

Figure 4 (cont.). Spatial distribution of long-term average monthly minimum air temperature for a) January, b) February, c) March, d) April, e) May, f) June, g) July, h) August, i) September, j) October, k) November and l) December.

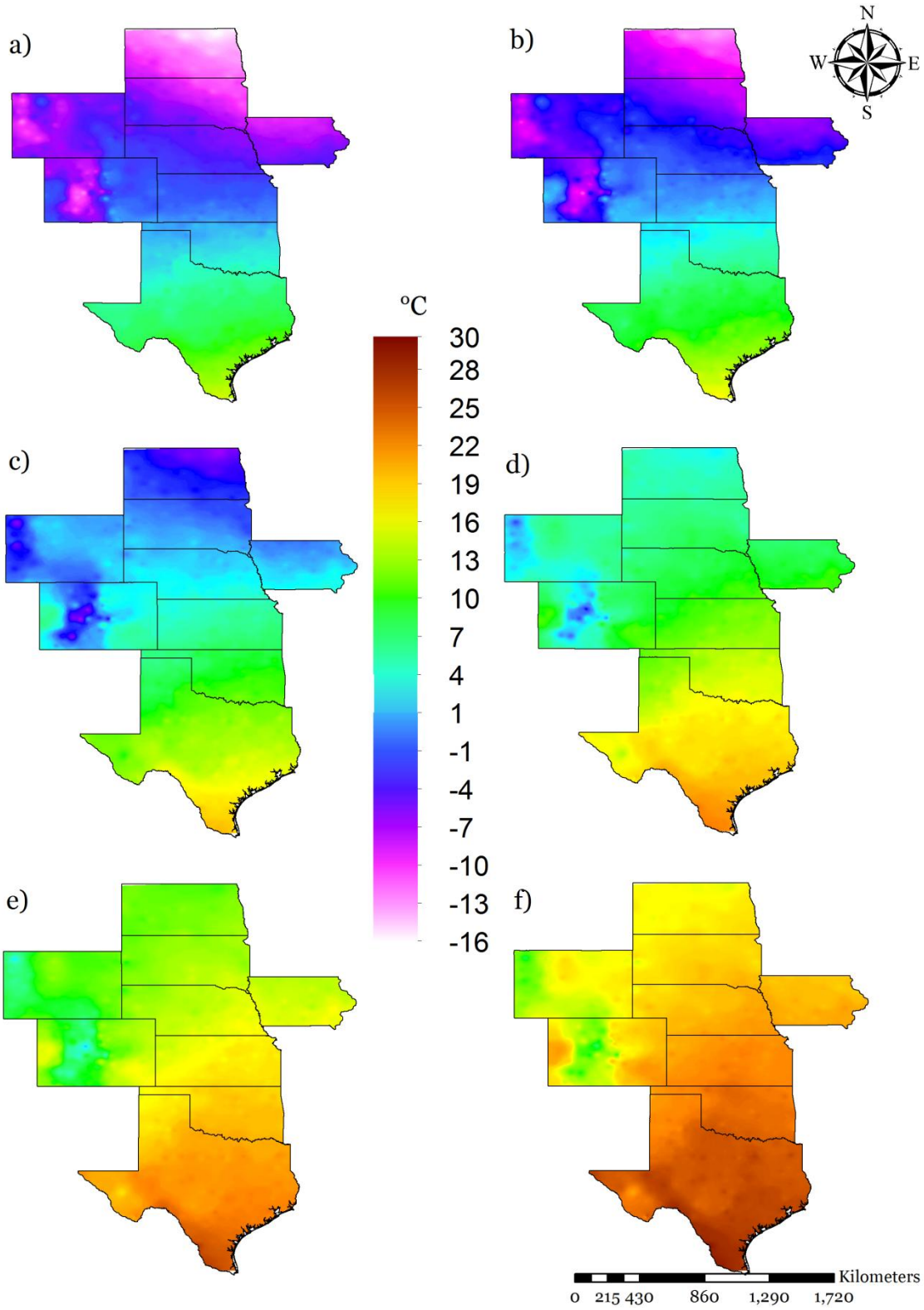

Figure 5. Spatial distribution of long-term average monthly mean air temperature for a) January, b) February, c) March, d) April, e) May, f) June, g) July, h) August, i) September, j) October, k) November and l) December.

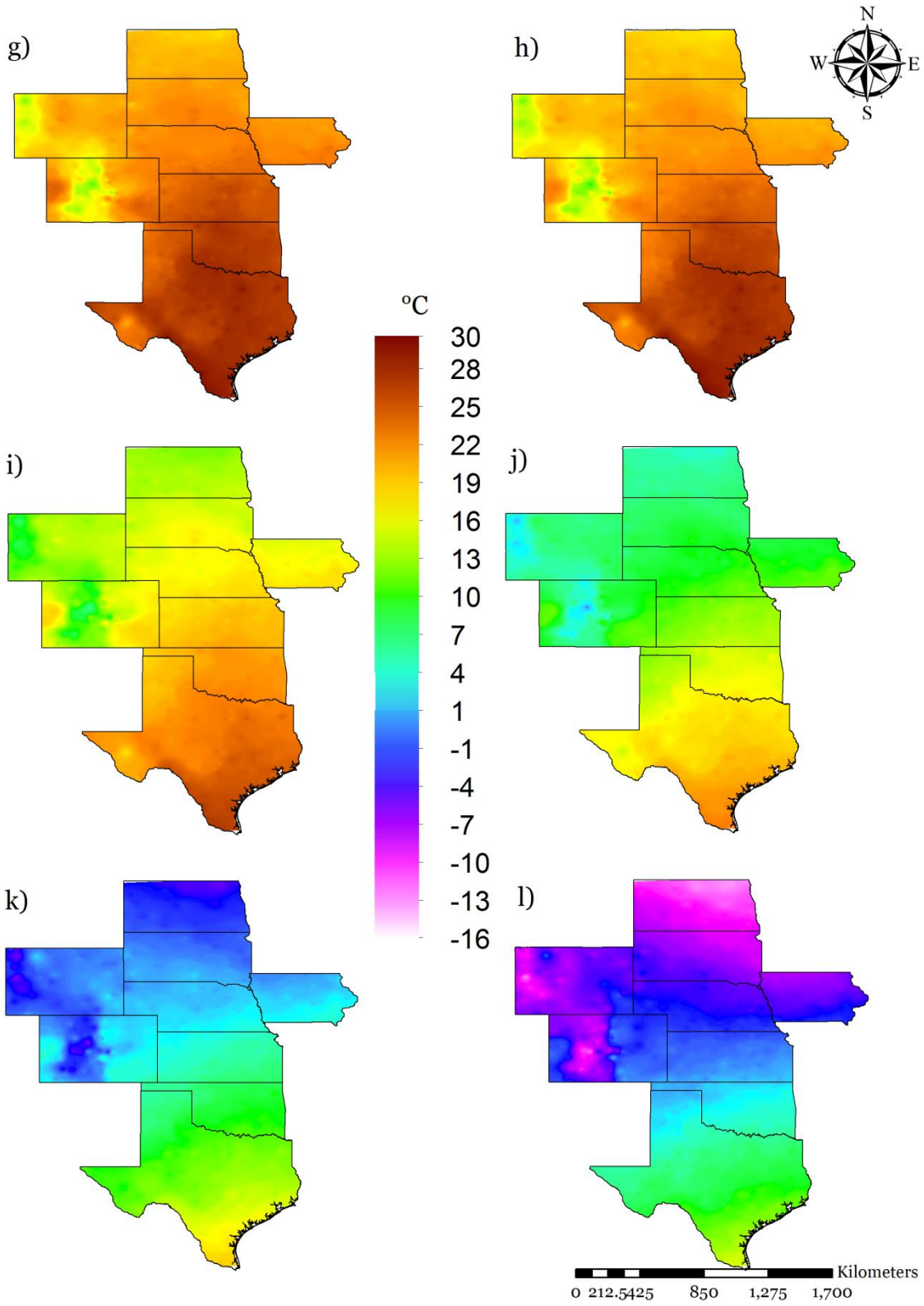

Figure 5 (cont.). Spatial distribution of long-term average monthly mean air temperature for a) January, b) February, c) March, d) April, e) May, f) June, g) July, h) August, i) September, j) October, k) November and l) December.

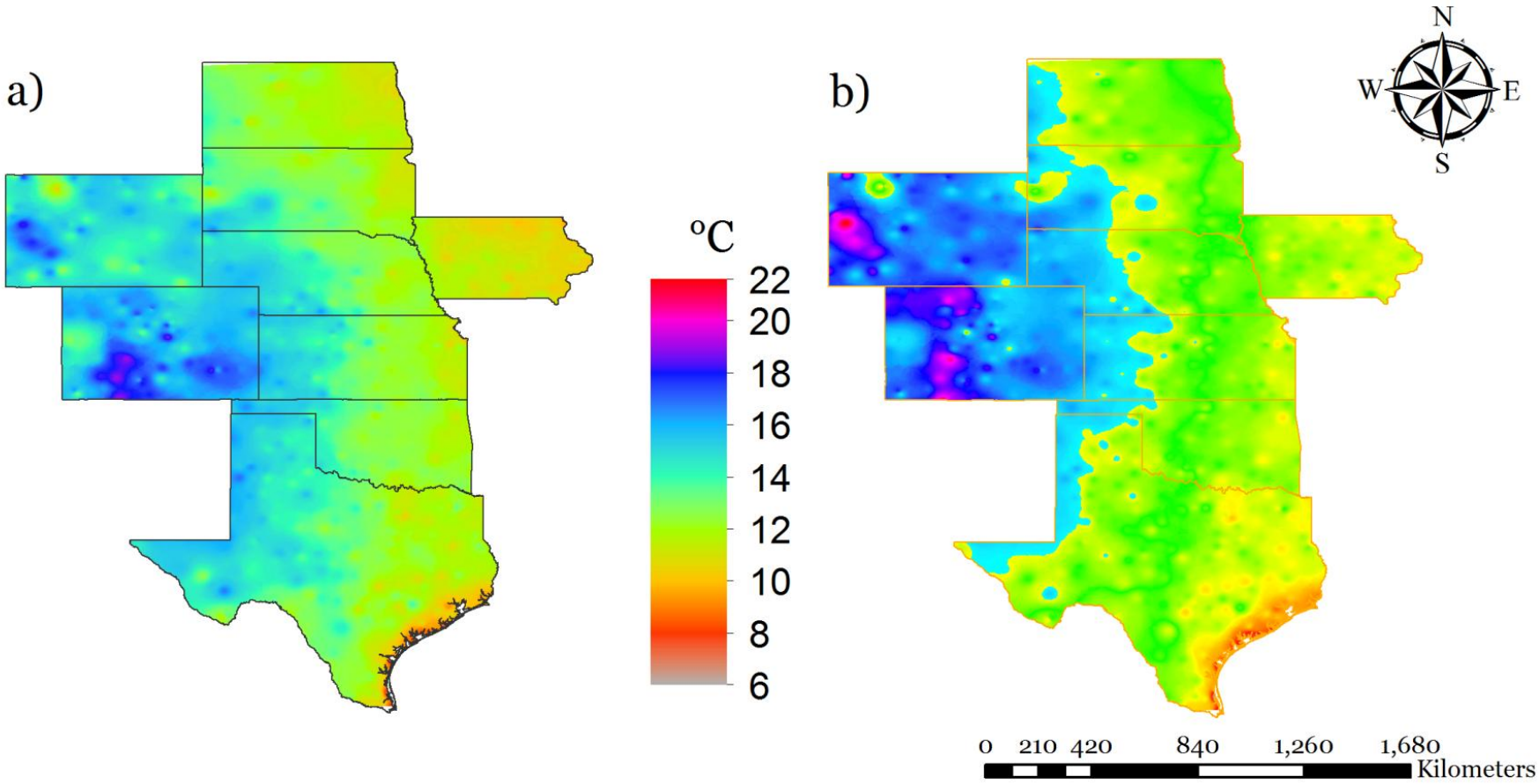

Figure 6. Spatial distribution of long-term average daily temperature range (DTR) on a) annual, b) growing season basis.

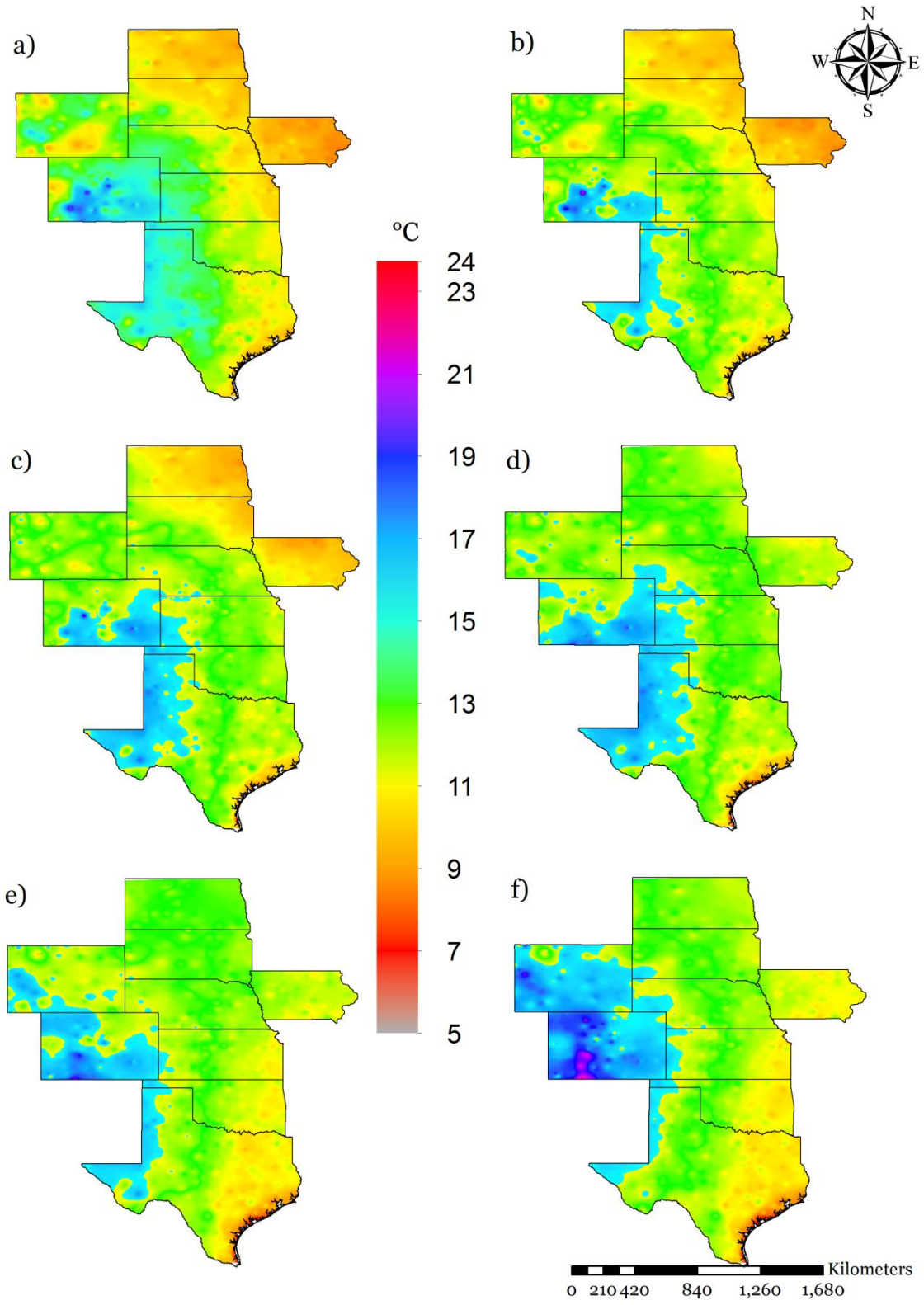

Figure 7. Spatial distribution of long-term average monthly daily temperature range (DTR) for a) January, b) February, c) March, d) April, e) May, f) June, g) July, h) August, i) September, j) October, k) November and l) December.

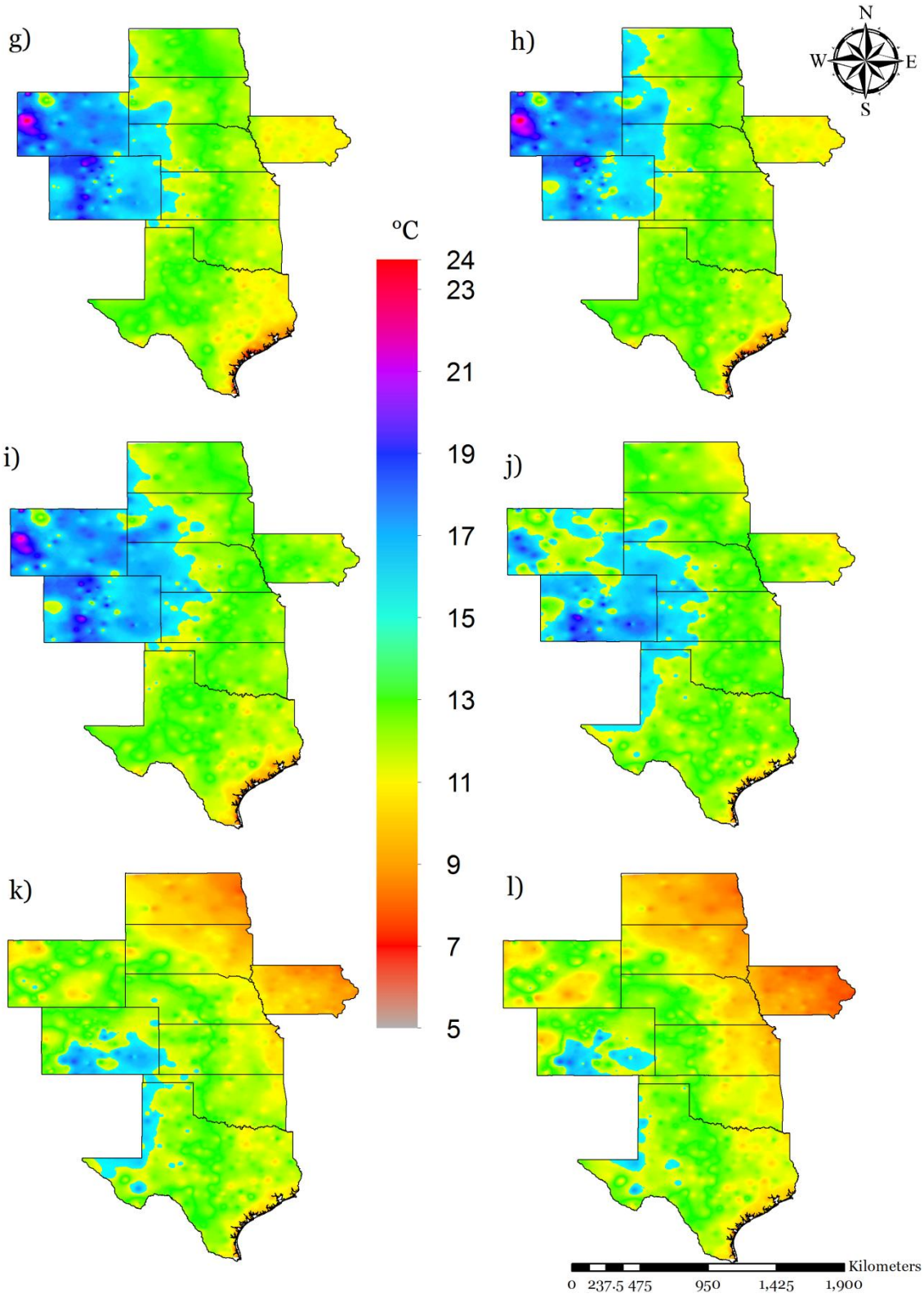

Figure 7 (cont.). Spatial distribution of long-term average monthly daily temperature range (DTR) for a) January, b) February, c) March, d) April, e) May, f) June, g) July, h) August, i) September, j) October, k) November and l) December.

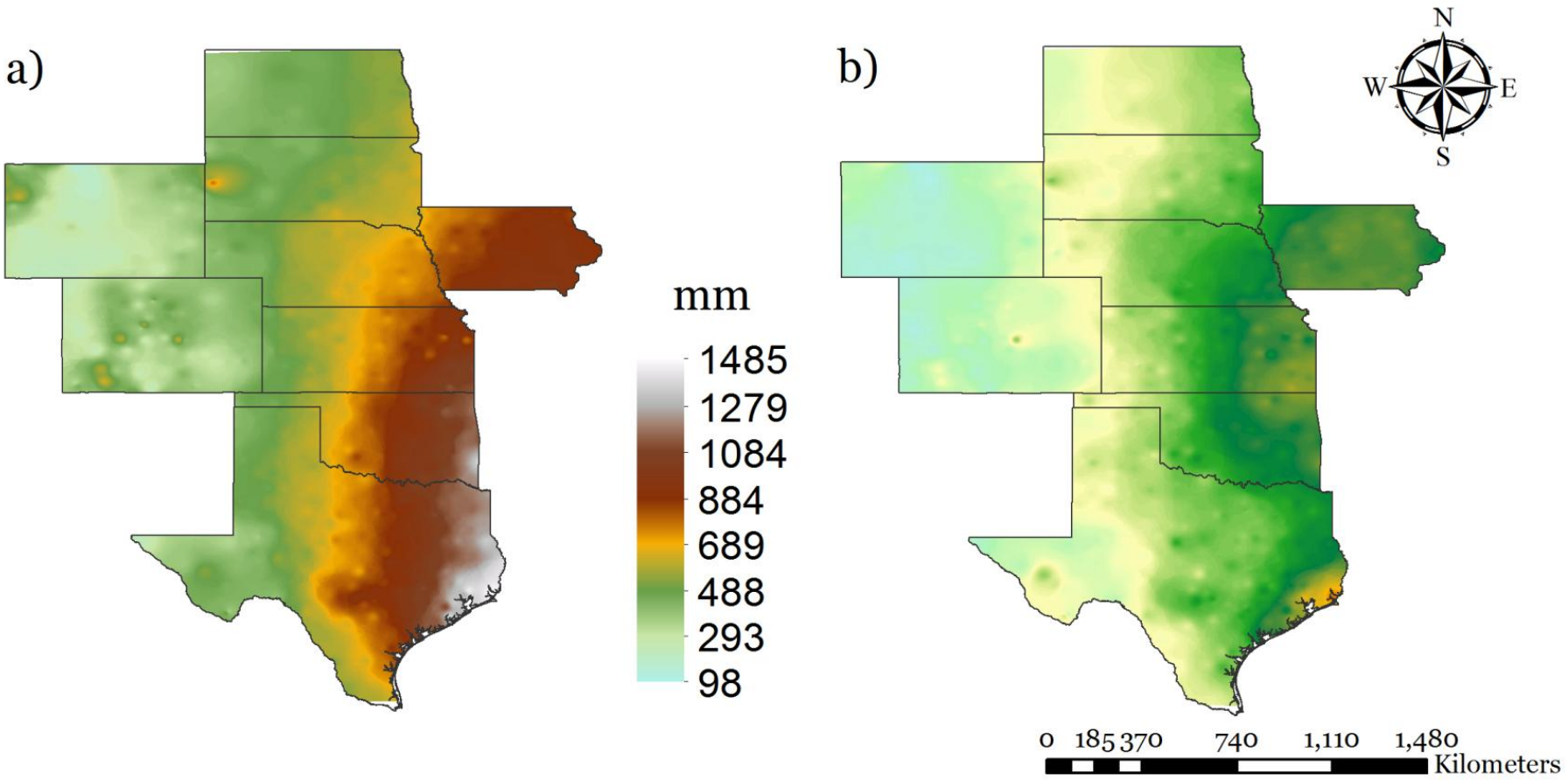

Figure 8. Spatial distribution of long-term average precipitation on a) annual, b) growing season basis.

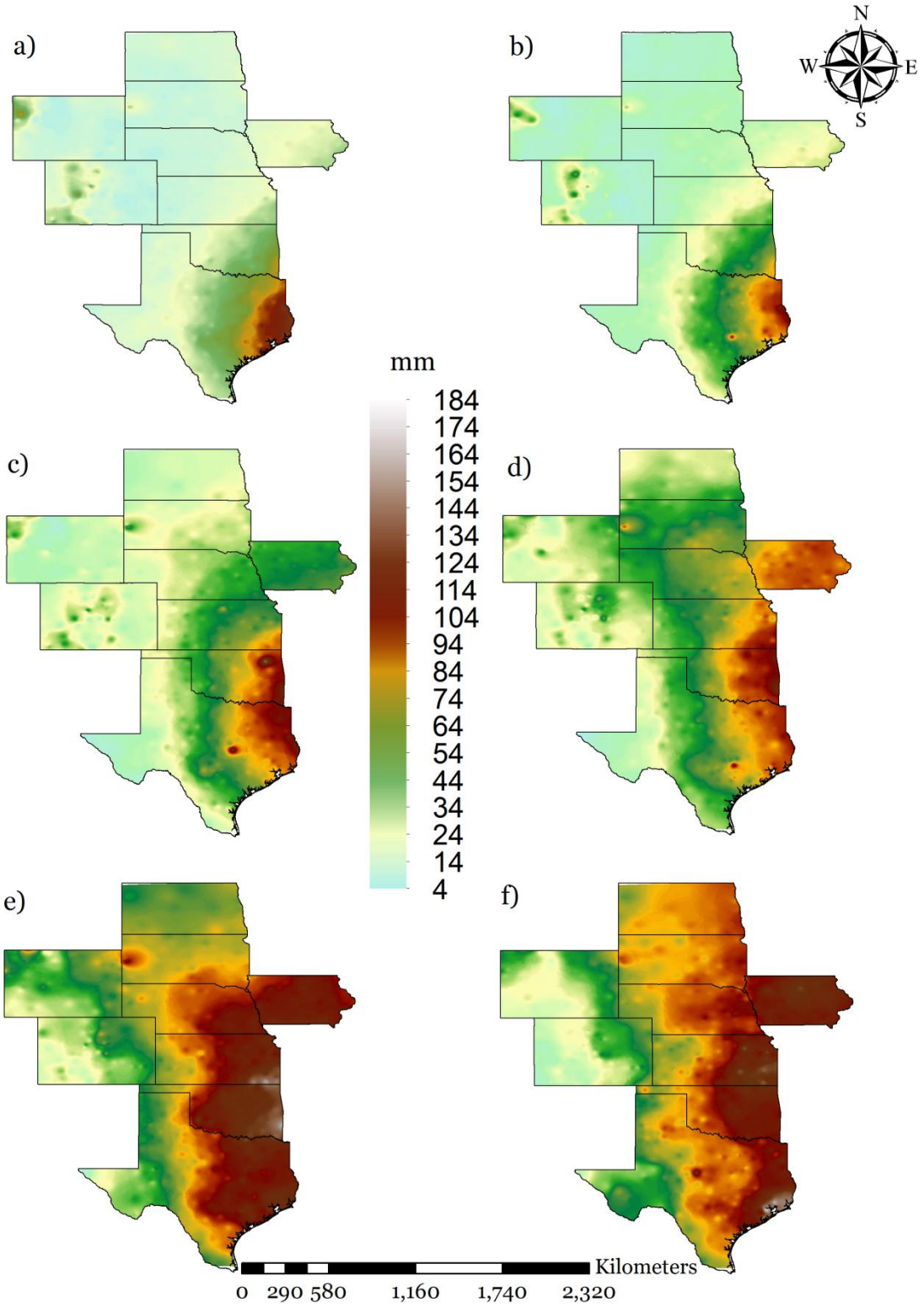

Figure 9. Spatial distribution of long-term average monthly precipitation for a) January, b) February, c) March, d) April, e) May, f) June, g) July, h) August, i) September, j) October, k) November and l) December.

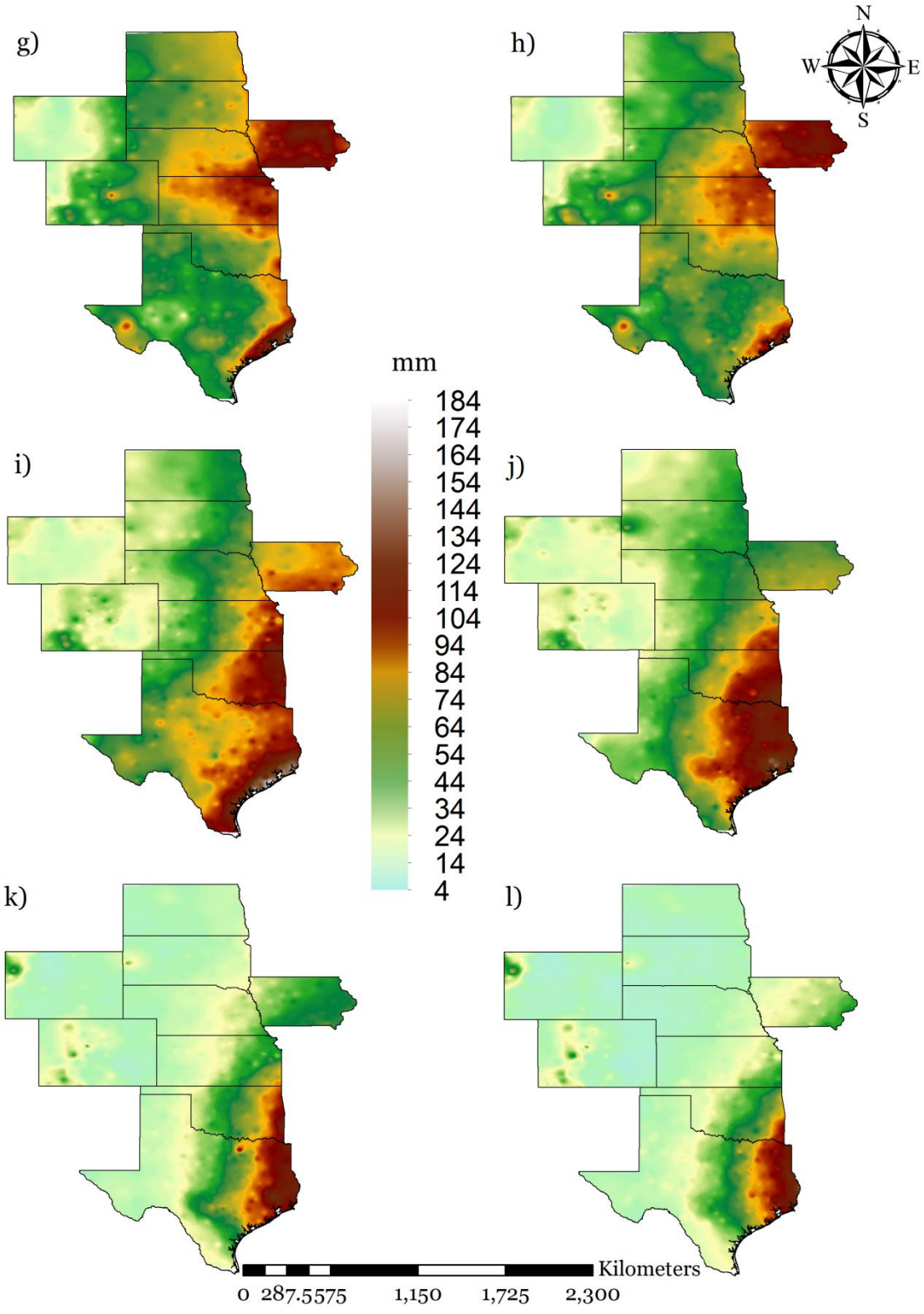

Figure 9 (cont.). Spatial distribution of long-term average monthly precipitation for a) January, b) February, c) March, d) April, e) May, f) June, g) July, h) August, i) September, j) October, k) November and l) December.

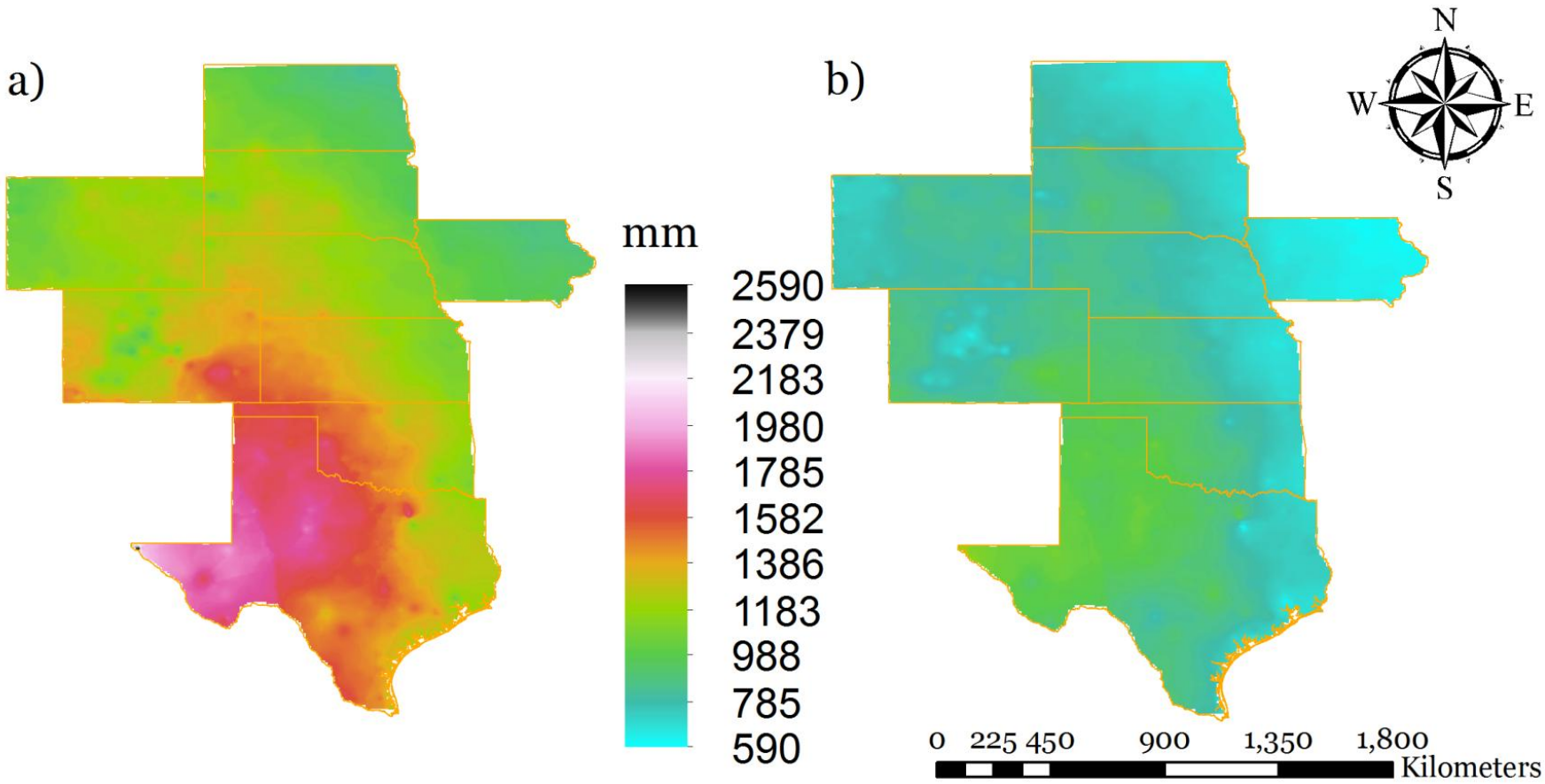

Figure 10. Spatial distribution of long-term average ET_o on a) annual, b) growing season basis.

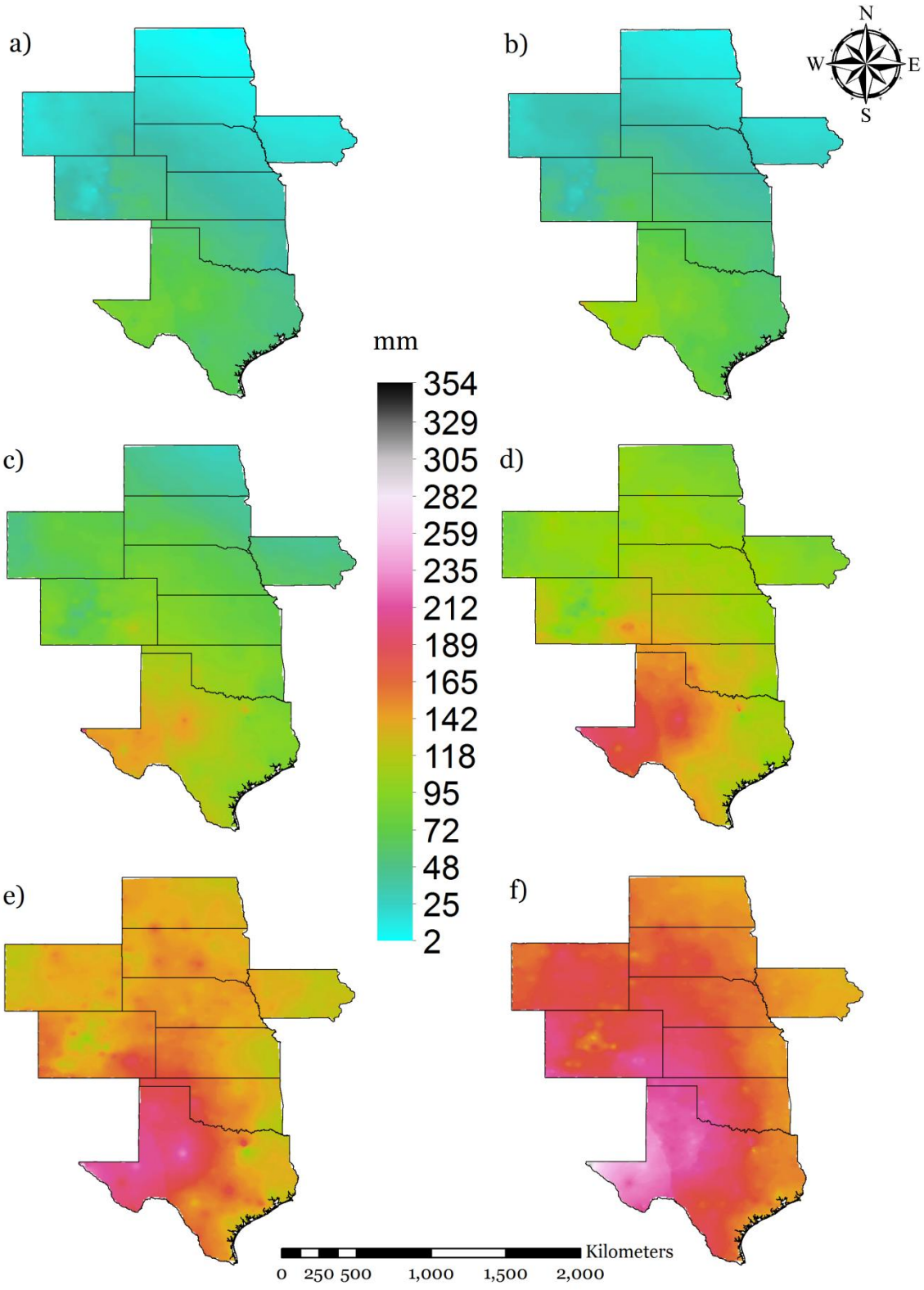

Figure 11. Spatial distribution of long-term average monthly ET_o for a) January, b) February, c) March, d) April, e) May, f) June, g) July, h) August, i) September, j) October, k) November and l) December.

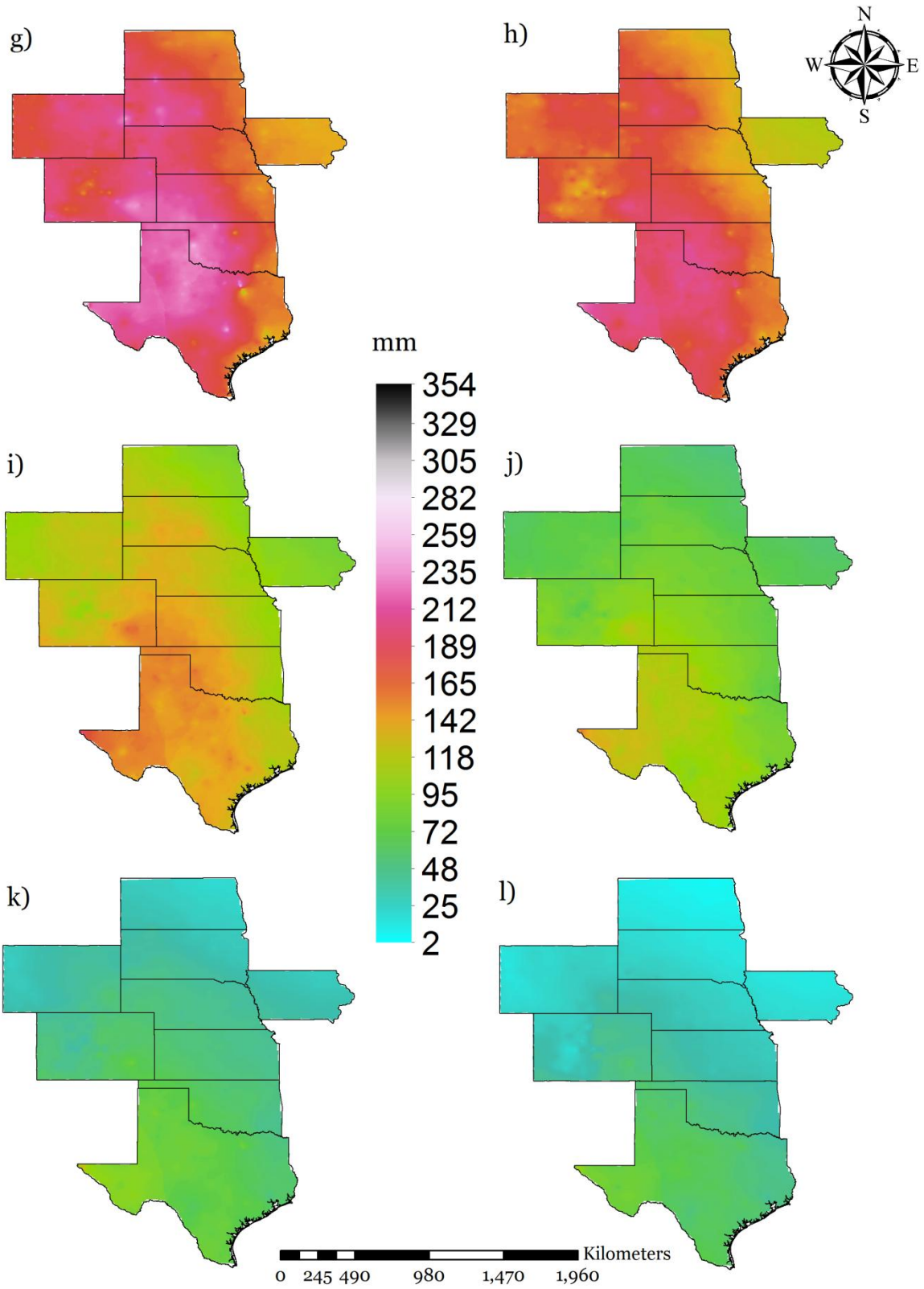

Figure 11 (cont.). Spatial distribution of long-term average monthly ET_o for a) January, b) February, c) March, d) April, e) May, f) June, g) July, h) August, i) September, j) October, k) November and l) December.

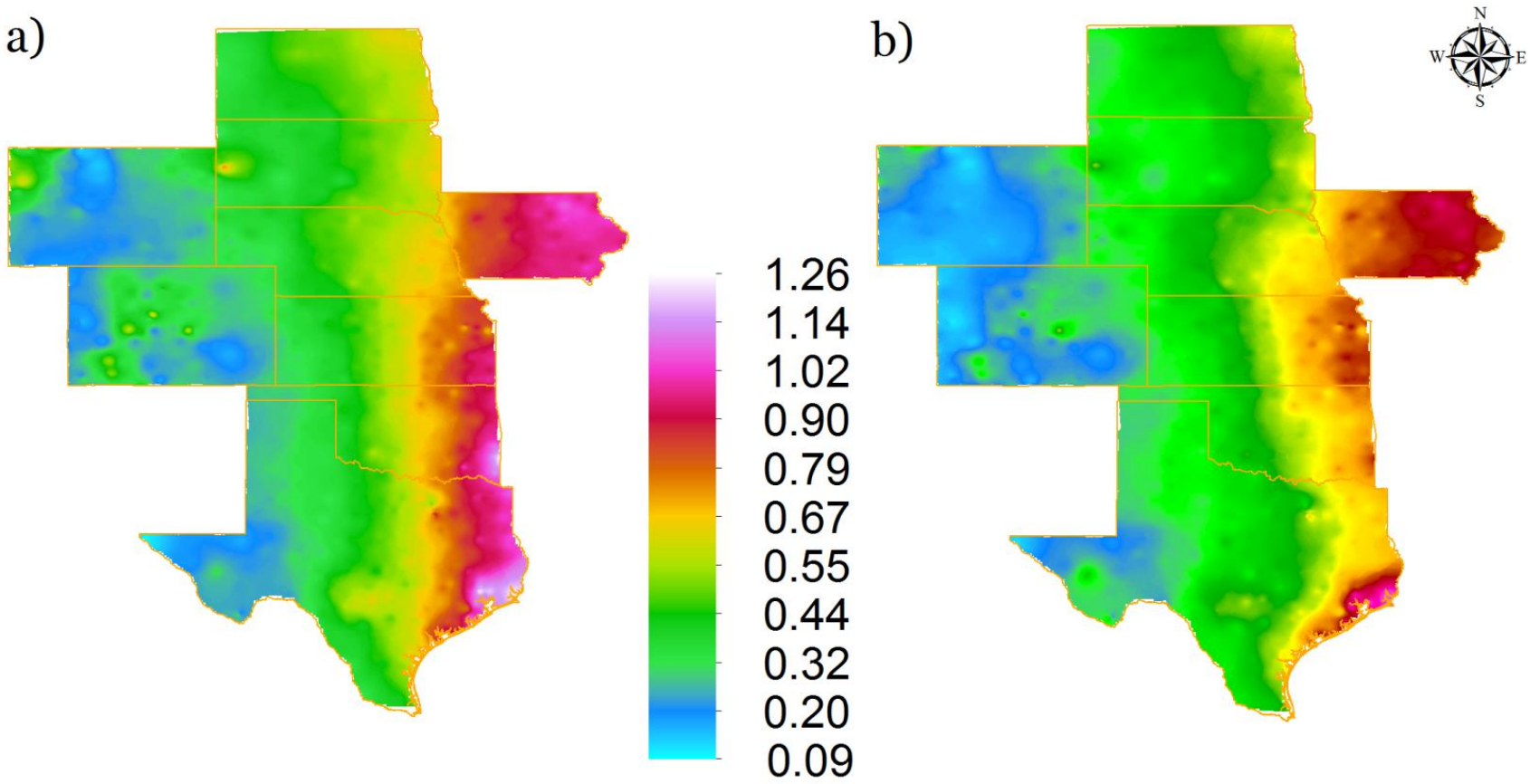

Figure 12. Spatial distribution of long-term average aridity index on a) annual, b) growing season basis.

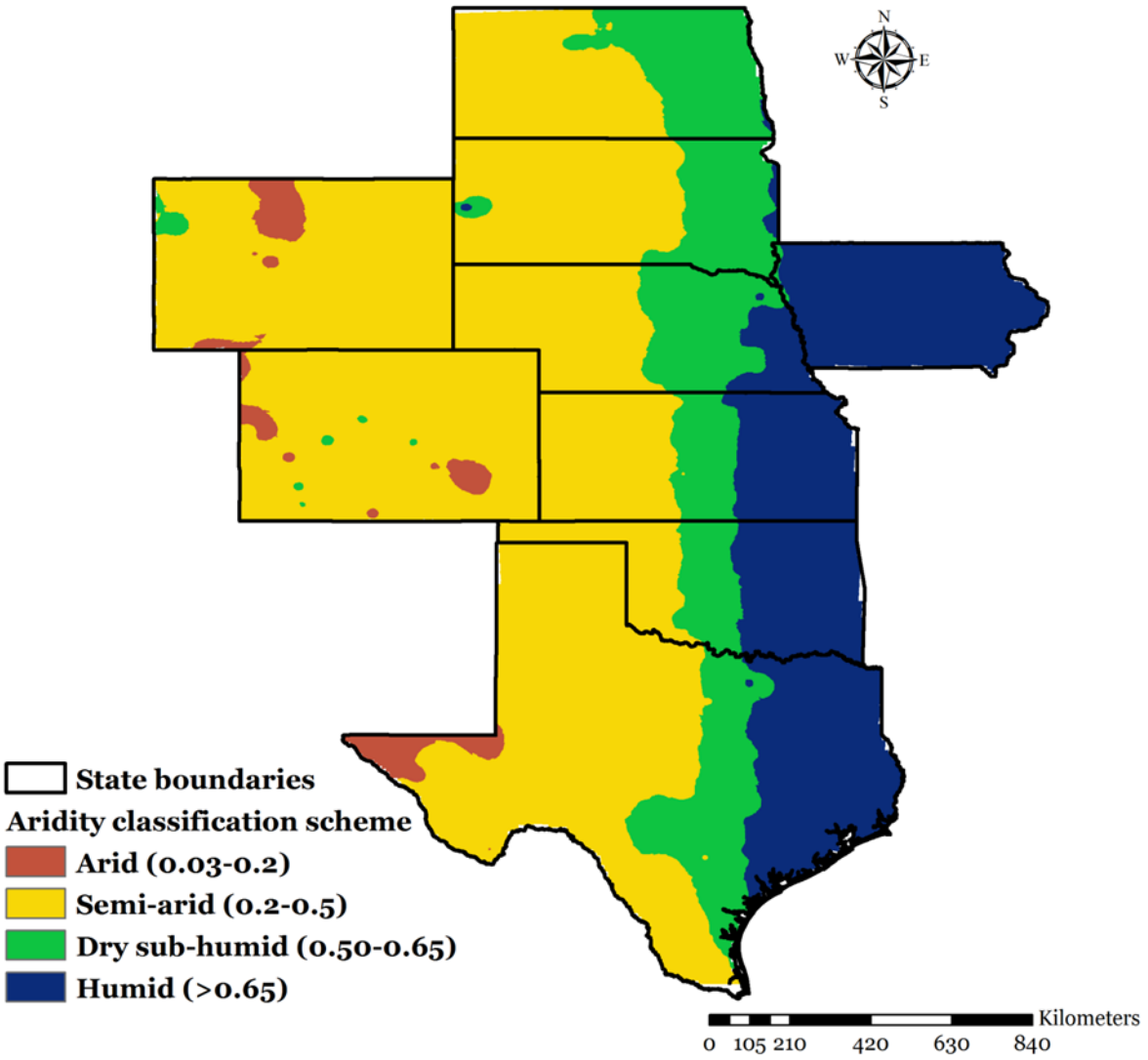

Figure 13. Classification of study region into aridity classes (UNEP, 1997)

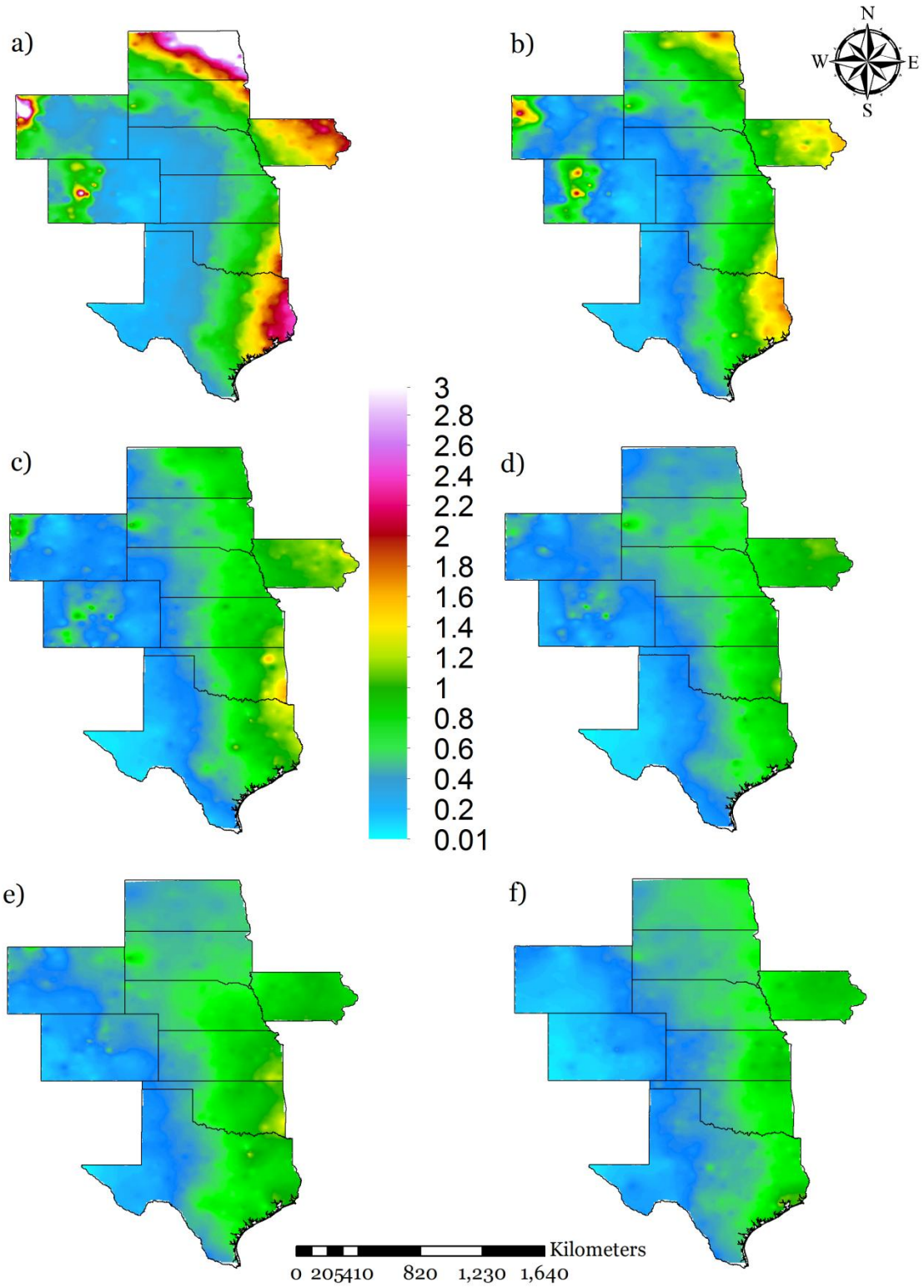

Figure 14. Spatial distribution of long-term average monthly aridity index (AI) for a) January, b) February, c) March, d) April, e) May, f) June, g) July, h) August, i) September, j) October, k) November and l) December.

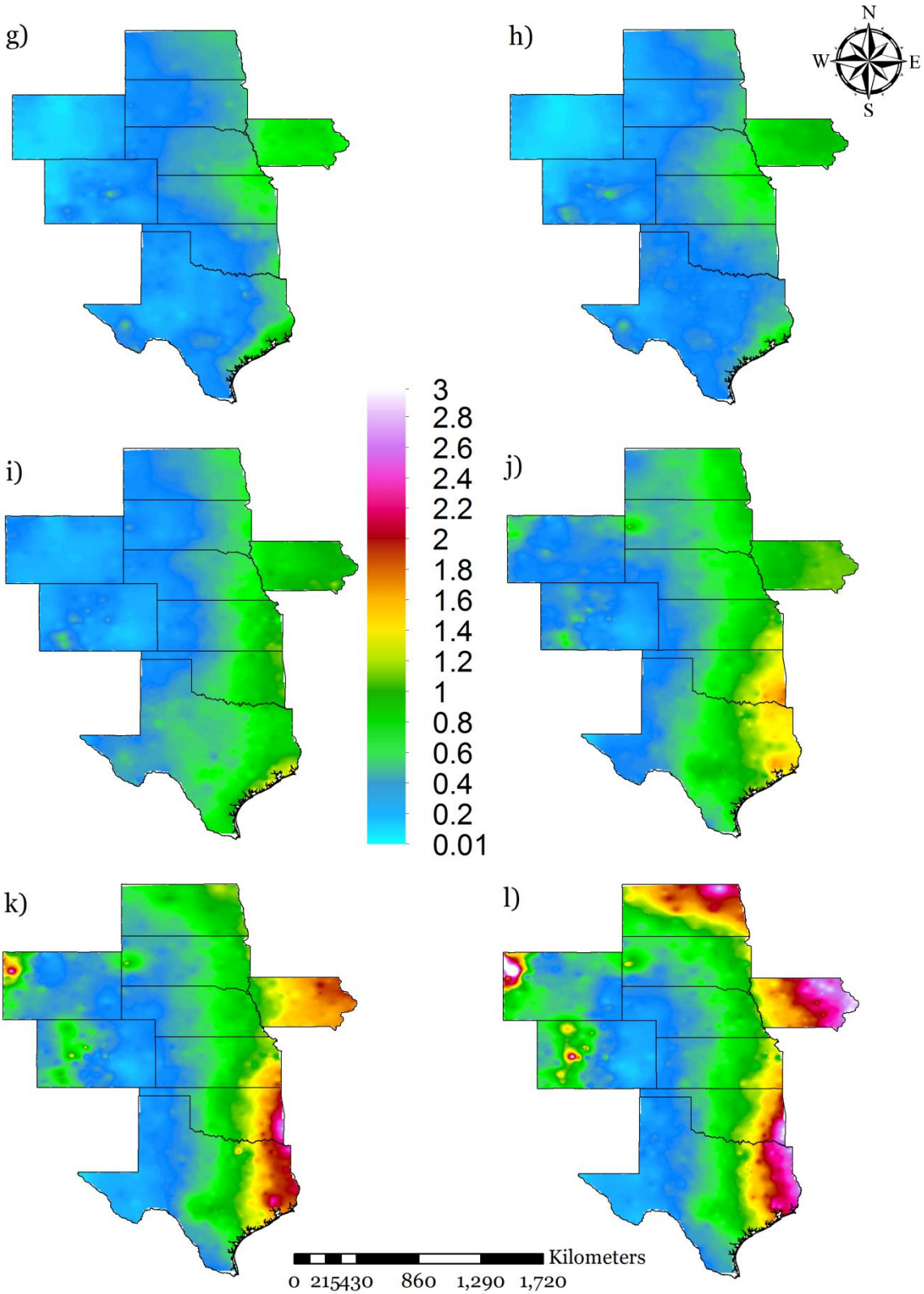

Figure 14 (cont.). Spatial distribution of long-term average monthly aridity index (AI) for a) January, b) February, c) March, d) April, e) May, f) June, g) July, h) August, i) September, j) October, k) November and l) December.